Oblate Spheroidal Kinematic Dynamos

D. J. Ivers
School of Mathematics & Statistics, University of Sydney, NSW 2006, Australia

May 30, 2017

Abstract

The kinematic dynamo problem is solved for a uniformly electrically-conducting fluid filling an oblate spheroidal volume with insulating exterior. The solution method uses a class of oblate spheroidal toroidal-poloidal fields in a non-orthogonal coordinate system. Scaling of coordinates and fields to a spherical geometry leads to a modified form of the kinematic dynamo problem with a geometric anisotropic diffusion and a modified current-free condition in the exterior, which must be solved explicitly. The scaling allows the use of well-developed spherical harmonic techniques in angle and large aspect ratios. Dynamo solutions are found for three axisymmetric flows in oblate spheroids with semi-axis ratios $1 \leq a/c \leq 25$. For larger aspect ratios strong magnetic fields may occur in any region of the spheroid, depending on the flow, but the external fields for all three flows are weak and concentrated near the axis or periphery of the spheroid.

Keywords: magnetohydrodynamics, dynamo theory, oblate spheroid, axisymmetric flow

1 Introduction

The generation of magnetic fields in the Earth, planets and stars can be modelled to a good approximation as self-exciting dynamos in electrically-conducting spherical or spherical shell cores with insulating exteriors. Fortunately, spheres and spherical shells are the bounded conductors with insulating exteriors, for which kinematic dynamos (Bullard and Gellman, 1954, Elsasser, 1946, Gubbins, 1973, Pekeris et al., 1973), and dynamically consistent dynamos (Glatzmaier and Roberts, 1995, Kageyama and Sato, 1995, Kuang and Bloxham, 1997), are the most mathematically and numerically tractable geometries, although still difficult (Christensen et al, 2001, Jackson et al, 2014, Jones et al., 2011, Jones, 2011, Marti et al, 2014, Matsui et al, 2016). The simplest aspherical geometry is spheroidal with one axis of arbitrary rotational symmetry. The Earth's core is a sphere at zeroth order and an oblate spheroid at second order, with finer-scale core-mantle boundary topography at higher orders. Spheroidal dynamos allow pressure coupling between the core and the mantle in dynamical dynamos and offer checks on methods for more general topography. Spheroidal dynamos of large semi-axis ratio, i.e. highly non-spherical, constitute an important class of dynamo geometries for elliptic and disk galaxies, and accretion disks; for example, E7-elliptical galaxies have major to minor semi-axis ratio $a/c = 10/3$. Galactic models are typically $\alpha\omega$-dynamos and use the thin disk approximation $a/c \to \infty$. See for example Stix (1975), White (1978), Soward (1978).

A spheroidal finite-element code has been developed by Wu and Roberts (2009), and finite-volume codes by Ernst-Hullermann et al. (2013) and Vantieghem et al. (2016). The aim of this work is to separately develop pseudo-spectral numerical solutions of the insulated kinematic dynamo problem (KDP), the rotating thermal convection problem and the rotating magneto-convection problem in spheroids and then to combine them to solve the dynamical dynamo problem. Pseudo-spectral codes generally perform more efficiently in spherical benchmarks for a given accuracy than finite-element and finite-volume codes (Christensen et al, 2001, Jackson et al, 2014, Jones et al., 2011, Marti et al, 2014, Matsui et al, 2016), but there is no best approach. A hybrid method for the insulated KDP is presented here, which is finite-difference in radius and Galerkin in angle. Galerkin or Cheychev collocation methods can also be used in radius.

The dynamo action of a moving electrically conducting fluid, which occupies an oblate spheroidal volume V in (Euclidean) space E^3, is considered. The velocity $\mathbf{v}$ of the fluid is prescribed. The volume V has semi-axes a and c ($a \geq c$), a rigid boundary Σ and is surrounded by an insulating exterior $E^3 \setminus V$. The magnetic induction field $\mathbf{B}$ is governed by the equations

$$\frac{\partial \mathbf{B}}{\partial t} = \nabla^2 \mathbf{B} + R_{\rm m} \nabla \times (\mathbf{v} \times \mathbf{B}) \quad \text{in } V; \quad \nabla \times \mathbf{B} = \mathbf{0} \quad \text{in } E^3 \setminus V; \quad \nabla \cdot \mathbf{B} = 0 \quad \text{in } E^3; \tag{1.1}$$

where the problem has been non-dimensionalised using a typical length $\mathcal{L}$, the magnetic diffusion time $\mathcal{L}^2/\eta$ and a typical speed $\mathcal{V}$ of the flow. The magnetic diffusivity η is uniform and $R_\mathrm{m} := \mathcal{V}\mathcal{L}/\eta$ is the magnetic Reynolds number. Useful choices for the length scale $\mathcal{L}$ are the major or minor semi-axes of the spheroidal boundary Σ, the radius of the sphere of volume $|V| = \frac{4}{3}\pi a^2 c$ or the radius of the circle of area πac, which imply respectively $a = 1$ and $0 < c \leq 1$, $c = 1$ and $1 \leq a < \infty$, $c = 1/a^2$ and $1 \leq a < \infty$ or $c = 1/a$ and $1 \leq a < \infty$. In cartesian coordinates (x, y, z) with the z-axis aligned along the symmetry axis of the spheroid, the boundary Σ and outward (non-unit) normal $\mathbf{n}$ are given by

$$\frac{x^2+y^2}{a^2} + \frac{z^2}{c^2} = 1\,, \quad \mathbf{n} := (x\mathbf{1}_x + y\mathbf{1}_y)/a^2 + z\mathbf{1}_z/c^2\,. \tag{1.2}$$

The vector field $\mathbf{n}$ is defined and smooth everywhere in E^3, not only on Σ. Besides the magnetic Reynolds number, a dimensionless shape parameter must be prescribed: the most useful are the aspect ratio a/c or its reciprocal, the flattening $f := 1 - c/a$ and the ellipticity $e := \sqrt{1-(c/a)^2}$. The flattening and ellipticity are related by $f = 1 - \sqrt{1-e^2}$ and $e = \sqrt{2f - f^2}$. Shape can also be parametrised by a semi-axis: if the volume is fixed so that $a^2c = 1$, then $a/c = a^3 = c^{-3/2}$ and $e = \sqrt{1-a^{-6}} = \sqrt{1-c^3}$; if $a = 1$ then $a/c = 1/c$ and $e = \sqrt{1-c^2}$; or if $c = 1$, then $a/c = a$ and $e = \sqrt{1-1/a^2}$.

The tangential components of $\mathbf{B}$ are continuous across Σ and $\mathbf{B}$ is self-exciting,

$$[\mathbf{n}\times\mathbf{B}]_\Sigma = \mathbf{0}\,, \quad [\mathbf{n}\cdot\mathbf{B}]_\Sigma = 0\,, \quad \mathbf{B} = \mathcal{O}(|\mathbf{r}|^{-3}) \quad \text{as } |\mathbf{r}| \to \infty, \tag{1.3}$$

where $[\,]_\Sigma$ denotes the jump outward across Σ and $\mathbf{r} = x\mathbf{1}_x + y\mathbf{1}_y + z\mathbf{1}_z$ is the radius vector from the origin. The flow $\mathbf{v}$ satisfies the mass conservation equation and the impenetrable boundary condition

$$\frac{\partial\rho}{\partial t} + R_\mathrm{m}\nabla\cdot(\rho\mathbf{v}) = 0\,, \quad \text{in } V\,; \qquad \mathbf{n}\cdot\mathbf{v} = 0\,, \quad \text{on } \Sigma. \tag{1.4}$$

If $\mathbf{v}$ is incompressible (1.4) reduces to

$$\nabla\cdot\mathbf{v} = 0\,, \quad \text{in } V. \tag{1.5}$$

In §2 classes of oblate spheroidal toroidal and poloidal fields analogous to the spherical classes are defined to reduce to two the number of fields necessary to represent a solenoidal magnetic field or an incompressible velocity. A further non-essential simplification is to scale the KDP to a spherical geometry. The spherically-scaled KDP produces equations with an anisotropic geometric magnetic diffusion in V, analogous to the anisotropic turbulent diffusion models considered by Phillips and Ivers (2000, 2003), and an anisotropic current-free condition in the insulating exterior. Numerical solution using spherical harmonic expansions in the homoeoidal angles [see (2.1)] analogous to the Bullard-Gellman equations (Bullard and Gellman, 1954) is described in §3. Results are given in §4 for magnetic free-decay and compared to the analytic solutions for aspect ratios $1 \leq a/c \leq 100$ in the axisymmetric case and small ellipticity in the non-axisymmetric case. Critical magnetic Reynolds numbers of three spheroidal dynamos also are found for $1 \leq a/c \leq 25$ based on three spherical axisymmetric dynamos of Dudley and James (1989). Alternative discretisations of the insulating exterior are considered in §5. Section 6 is the conclusion.

2 A Class of Oblate Spheroidal Toroidal-Poloidal Fields

Introduce homeoidal oblate ($a \geq c$) spheroidal coordinates (r, θ, ϕ)

$$x = ar\sin\theta\ \cos\phi\,, \quad y = ar\sin\theta\ \sin\phi\,, \quad z = cr\cos\theta\ . \tag{2.1}$$

where $0 \leq r < \infty$, $0 \leq \theta \leq \pi$ and ϕ is the azimuthal angle. Note: r is *not* $|\mathbf{r}|$. If (r, θ, ϕ) are the coordinates of a point $P(x, y, z)$, then P lies on the oblate spheroidal r-surface $\Sigma(r)$,

$$\frac{x^2+y^2}{a^2} + \frac{z^2}{c^2} = r^2\,.$$

Moreover, if Q is the projection of P parallel to the z-axis, onto the sphere of radius ar escribed on the spheroid, then θ is the angle $\angle zOQ$. The spheroid (1.2) corresponds to $r = 1$, i.e. $\Sigma(1)$ is Σ. The meridional sections of the r-surfaces are concentric homeoidal ellipses of equal ellipticity e. Their foci lie on the azimuthal circle of radius aer in the equatorial plane $z = 0$, so the $\Sigma(r)$ are not confocal, and $aer \to 0$ as $r \to 0$.

The coordinate system (r,θ,ϕ) is not orthogonal if $a \neq c$. There are two reciprocal sets of basis vectors associated with (r,θ,ϕ), the covariant basis $(\mathbf{e}_1,\mathbf{e}_2,\mathbf{e}_3) := (\partial_r\mathbf{r},\partial_\theta\mathbf{r},\partial_\phi\mathbf{r})$, and the contravariant basis $(\mathbf{e}^1,\mathbf{e}^2,\mathbf{e}^3) := (\nabla r,\nabla\theta,\nabla\phi)$. The bases $(\mathbf{e}_1,\mathbf{e}_2,\mathbf{e}_3)$ and $(\mathbf{e}^1,\mathbf{e}^2,\mathbf{e}^3)$ are related by the usual reciprocity relations, $\mathbf{e}_i = \frac{1}{2}J\epsilon_{ijk}\mathbf{e}^j \times \mathbf{e}^k$ and $\mathbf{e}^i = \frac{1}{2}J^{-1}\epsilon^{ijk}\mathbf{e}_j \times \mathbf{e}_k$, where $J = \partial(x,y,z)/\partial(r,\theta,\phi) = a^2 c\, r^2 \sin\theta$ is the Jacobian of the transformation (2.1), repeated indices are summed and ϵ_{ijk}, ϵ^{ijk} are the unit rank-3 alternating tensors. The bases satisfy the bi-orthogonality condition, $\mathbf{e}_i \cdot \mathbf{e}^j = \delta_i^j$. At any point on $\Sigma(r)$, $\mathbf{e}^1$ is normal to $\Sigma(r)$, and $\mathbf{e}_2$ and $\mathbf{e}_3$ are tangential; $\mathbf{e}_1$ is not parallel to $\mathbf{e}^1$ and hence not normal to $\Sigma(r)$ except along principal axes. In fact, $\mathbf{n} = \nabla\frac{1}{2}r^2 = r\mathbf{e}^1$. The vector element of surface area on $\Sigma(r)$ is $\mathrm{d}\boldsymbol{\Sigma}(r) = \mathbf{e}_2 \times \mathbf{e}_3\,\mathrm{d}\theta\,\mathrm{d}\phi = J\mathbf{e}^1\,\mathrm{d}\theta\,\mathrm{d}\phi = \mathbf{n}\,a^2 c\, r\sin\theta\,\mathrm{d}\theta\,\mathrm{d}\phi$ and $\mathrm{d}\Sigma(r) = |\mathbf{n}|\,a^2 c\, r\sin\theta\,\mathrm{d}\theta\,\mathrm{d}\phi$. The volume element $\mathrm{d}V = a^2 c\, r^2\sin\theta\,\mathrm{d}r\,\mathrm{d}\theta\,\mathrm{d}\phi = |\mathbf{n}|^{-1}\mathrm{d}\Sigma(r) r\,\mathrm{d}r$. The operator $\nabla = \mathbf{e}^1\partial_r + \mathbf{e}^2\partial_\theta + \mathbf{e}^3\partial_\phi$.

The two bases have the important derivative properties, $\nabla\cdot(J^{-1}\mathbf{e}_i) = 0$ and $\nabla\times\mathbf{e}^i = \mathbf{0}$. Thus, the divergence of a vector field $\mathbf{F}$ in terms of its contravariant components, $\mathbf{F} = F^1\mathbf{e}_1 + F^2\mathbf{e}_2 + F^3\mathbf{e}_3$, is given by

$$\nabla\cdot\mathbf{F} = J^{-1}\{\partial_r(JF^1) + \partial_\theta(JF^2) + \partial_\phi(JF^3)\}\,.$$

Let $\mathbf{e}_r := \mathbf{e}_1$, $\mathbf{e}_\theta := \mathbf{e}_2/r$, $\mathbf{e}_\phi := \mathbf{e}_3/r\sin\theta$ and $\mathbf{B} = B_r\mathbf{e}_r + B_\theta\mathbf{e}_\theta + B_\phi\mathbf{e}_\phi$, then $\mathbf{B}$ is solenoidal if and only if $\partial_r(r^2\sin\theta\,B_r) + \partial_\theta(r\sin\theta\,B_\theta) + \partial_\phi(r\,B_\phi) = 0$. By analogy with spherical polar coordinates, *homoeoidal oblate spheroidal toroidal* and *poloidal fields* can be defined component-wise by

$$\mathbf{T}\{T\} := \mathbf{e}_\theta\,\frac{\partial_\phi T}{\sin\theta} - \mathbf{e}_\phi\,\partial_\theta T\,, \qquad \mathbf{S}\{S\} := -\mathbf{e}_r\,\frac{\mathring{\Lambda}^2 S}{r} + \mathbf{e}_\theta\,\frac{\partial_\theta\partial_r(rS)}{r} + \mathbf{e}_\phi\,\frac{\partial_\phi\partial_r(rS)}{r\sin\theta}\,, \tag{2.2}$$

where $\sin^2\theta\,\mathring{\Lambda}^2 S = \sin\theta\,\partial_\theta(\sin\theta\,\partial_\theta S) + \partial_\phi\partial_\phi S$, such that $\nabla\cdot\mathbf{T}\{T\} = 0$ and $\nabla\cdot\mathbf{S}\{S\} = 0$. The magnetic field can thus be represented in E^3 as a sum of oblate-spheroidal toroidal and poloidal fields, $\mathbf{B} = \mathbf{T}\{T\} + \mathbf{S}\{S\}$. For any T, S and $r > 0$ the fields $\mathbf{T}\{T\}$ and $\mathbf{S}\{S\}$ are orthogonal over $\Sigma(r)$ in a certain sense; see equation (2.9) below. The matching and self-exciting conditions (1.3) become

$$[S]_\Sigma = 0\,, \quad [\partial_r S]_\Sigma = 0\,, \quad [T]_\Sigma = 0\,; \qquad S = \mathcal{O}(r^{-2})\,, \quad T = \mathcal{O}(r^{-3}) \quad \text{as } r\to\infty. \tag{2.3}$$

Note that, since $a^2 c\mathbf{e}^2\times\mathbf{e}^3 = \mathbf{e}_r/r^2\sin\theta$, $a^2 c\mathbf{e}^3\times\mathbf{e}^1 = \mathbf{e}_\theta/r\sin\theta$, $a^2 c\mathbf{e}^1\times\mathbf{e}^2 = \mathbf{e}_\phi/r$,

$$\mathbf{T}\{T\} = \nabla\times a^2 c(T\nabla\tfrac{1}{2}r^2) = \nabla T\times a^2 c\mathbf{n}\,, \quad \mathbf{S}\{S\} = \nabla\times a^2 c\bigg(\frac{r\partial_\phi S}{\sin\theta}\mathbf{e}^2 - r\sin\theta\,\partial_\theta S\mathbf{e}^3\bigg)\,.$$

In particular, $\mathbf{n}\cdot\mathbf{T}\{T\} = 0$. Typically, $\nabla\times\mathbf{T}\{T\} \neq \mathbf{S}\{S\}$ for any S and $\nabla\times\mathbf{S}\{S\} \neq \mathbf{T}\{T\}$ for any T. Physically, an oblate spheroidal toroidal (poloidal) magnetic field does not generate, nor is generated by, a purely oblate spheroidal poloidal (toroidal) electric current. If incompressible the velocity can also be represented as a sum of oblate spheroidal toroidal and poloidal fields, $\mathbf{v} = \mathbf{T}\{t\} + \mathbf{S}\{s\}$, with potentials t and s. (Only in ∂_t and $e^{\gamma t}$ does t represent the time.)

2.1 Spherically-Scaled Coordinates and Fields

It is possible to proceed in the basis $(\mathbf{e}_r,\mathbf{e}_\theta,\mathbf{e}_\phi)$, but it is easier to scale the cartesian coordinates, $\mathring{x} = x/a$, $\mathring{y} = y/a$ and $\mathring{z} = z/c$, and the components of the magnetic field and the velocity along principal axes of the spheroid (1.2),

$$\mathring{\mathbf{r}} = \mathbf{L}\cdot\mathbf{r} = \mathbf{r}\cdot\mathbf{L}\,, \quad \mathring{\nabla} = \mathbf{L}^{-1}\cdot\nabla\,, \quad \mathring{\mathbf{B}} = \mathbf{L}\cdot\mathbf{B} = \mathbf{B}\cdot\mathbf{L}\,, \quad \mathring{\mathbf{v}} = \mathbf{L}\cdot\mathbf{v} = \mathbf{v}\cdot\mathbf{L}\,, \quad \mathbf{n} = \mathbf{L}\cdot\mathring{\mathbf{r}}\,, \tag{2.4}$$

where $\mathring{\mathbf{r}} := \mathring{x}\mathbf{1}_x + \mathring{y}\mathbf{1}_y + \mathring{z}\mathbf{1}_z$ is the position vector in $(\mathring{x},\mathring{y},\mathring{z})$-space $\mathring{E}^3$, the diagonal scale tensor $\mathbf{L} := a^{-1}(\mathbf{1}_x\mathbf{1}_x + \mathbf{1}_y\mathbf{1}_y) + c^{-1}\mathbf{1}_z\mathbf{1}_z$ with inverse $\mathbf{L}^{-1} := a(\mathbf{1}_x\mathbf{1}_x + \mathbf{1}_y\mathbf{1}_y) + c\mathbf{1}_z\mathbf{1}_z$ and the operator $\mathring{\nabla} := \mathbf{1}_x\partial_{\mathring{x}} + \mathbf{1}_y\partial_{\mathring{y}} + \mathbf{1}_z\partial_{\mathring{z}}$. The transformation is not simply a (passive) change of variable on the manifold E^3, since the same cartesian unit vectors are used in $\mathring{E}^3$: $(\mathbf{1}_{\mathring{x}},\mathbf{1}_{\mathring{y}},\mathbf{1}_{\mathring{z}}) = (\mathbf{1}_x,\mathbf{1}_y,\mathbf{1}_z)$. The scale tensor $\mathbf{L}$ can be separated into isotropic and anisotropic parts,

$$\mathbf{L} = \frac{1}{a}\Big(\mathbf{I} + \frac{f}{1-f}\mathbf{1}_z\mathbf{1}_z\Big)\,, \quad \mathbf{L}^{-1} = a(\mathbf{I} - f\mathbf{1}_z\mathbf{1}_z)\,, \tag{2.5}$$

where $\mathbf{I}$ is the identity tensor. Note $|\mathring{\mathbf{r}}| = r$ and $\mathring{\Lambda}^2 = \mathring{\boldsymbol{\Lambda}}\cdot\mathring{\boldsymbol{\Lambda}}$ where $\mathring{\boldsymbol{\Lambda}} := \mathring{\mathbf{r}}\times\mathring{\nabla}$. The stretching transforms the r-surface $\Sigma(r)$ from a spheroid into a sphere $\mathring{\Sigma}(r)$ of radius in $\mathring{E}^3$; the image $\mathring{V}$ of the conducting fluid region

V under the transformation is the sphere $r < 1$ and the image of its boundary Σ is the unit sphere $\mathring{\Sigma} = \mathring{\Sigma}(1)$ with normal $\mathring{\mathbf{n}} = \mathring{\mathbf{r}}$. The volume element $\mathrm{d}V = \partial(x,y,z)/\partial(\mathring{x},\mathring{y},\mathring{z})\mathrm{d}\mathring{x}\,\mathrm{d}\mathring{y}\,\mathrm{d}\mathring{z} = a^2 c\,\mathrm{d}\mathring{V}$. Poincaré (1885) and Bryan (1889) used this device in the study of the equilibrium of rotating, self-gravitating homogeneous liquids. In general equations (2.4) imply

$$\nabla\cdot\mathbf{B} = \mathring{\nabla}\cdot\mathring{\mathbf{B}},\ \nabla\cdot\mathbf{v} = \mathring{\nabla}\cdot\mathring{\mathbf{v}};\ \mathbf{B}\cdot\nabla = \mathring{\mathbf{B}}\cdot\mathring{\nabla},\ \mathbf{v}\cdot\nabla = \mathring{\mathbf{v}}\cdot\mathring{\nabla};\ \mathbf{n}\cdot\mathbf{B} = \mathring{\mathbf{r}}\cdot\mathring{\mathbf{B}},\ \mathbf{n}\cdot\mathbf{v} = \mathring{\mathbf{r}}\cdot\mathring{\mathbf{v}}\,. \tag{2.6}$$

The variables (r,θ,ϕ) introduced in (2.1) are spherical polar coordinates in $\mathring{E}^3$. The basis $(\mathbf{e}_r,\mathbf{e}_\theta,\mathbf{e}_\phi)$ in E^3 is transformed into the orthonormal spherical polar basis $(\mathbf{1}_r,\mathbf{1}_\theta,\mathbf{1}_\phi) = \mathbf{L}\cdot(\mathbf{e}_r,\mathbf{e}_\theta,\mathbf{e}_\phi)$ in $\mathring{E}^3$. Thus the scalar components of $\mathring{\mathbf{B}} = \mathring{B}_r\mathbf{1}_r + \mathring{B}_\theta\mathbf{1}_\theta + \mathring{B}_\phi\mathbf{1}_\phi$ and $\mathbf{B}$ with respect to $(\mathbf{e}_r,\mathbf{e}_\theta,\mathbf{e}_\phi)$ are equal, $\mathring{B}_r = B_r$ $\mathring{B}_\theta = B_\theta$ and $\mathring{B}_\phi = B_\phi$, but different with respect to $(\mathbf{1}_x,\mathbf{1}_y,\mathbf{1}_z)$. Hence the oblate spheroidal toroidal-poloidal representation for the magnetic field becomes

$$\mathring{\mathbf{B}} = \mathbf{L}\cdot(\mathbf{T}\{T\} + \mathbf{S}\{S\}) = \mathring{\mathbf{T}}\{T\} + \mathring{\mathbf{S}}\{S\} = \mathring{\nabla}\times T\mathring{\mathbf{r}} + \mathring{\nabla}\times\mathring{\nabla}\times S\mathring{\mathbf{r}}\,. \tag{2.7}$$

Thus oblate spheroidal toroidal (poloidal) fields are scaled to spherical toroidal (poloidal) fields in $\mathring{E}^3$,

$$\mathring{\mathbf{T}}\{T\} = \mathbf{1}_\theta\,\frac{\partial_\phi T}{\sin\theta} - \mathbf{1}_\phi\,\partial_\theta T\,,\qquad \mathring{\mathbf{S}}\{S\} = -\mathbf{1}_r\,\frac{\mathring{\Lambda}^2 S}{r} + \mathbf{1}_\theta\,\frac{\partial_\theta\partial_r(rS)}{r} + \mathbf{1}_\phi\,\frac{\partial_\phi\partial_r(rS)}{r\sin\theta}\,, \tag{2.8}$$

The conditions $\oint S\,\mathrm{d}\mathring{\Omega} = 0$ and $\oint T\,\mathrm{d}\mathring{\Omega} = 0$, where $\mathrm{d}\mathring{\Omega} := \sin\theta\,\mathrm{d}\theta\,\mathrm{d}\phi$ is the element of solid angle on $\mathring{\Sigma}(r)$, are imposed to ensure uniqueness of S and T. For all T, S and $r > 0$, $\mathring{\mathbf{T}}\{T\}$ and $\mathring{\mathbf{S}}\{S\}$ are orthogonal on $\mathring{\Sigma}(r)$,

$$\oint \mathbf{T}\{T\}\cdot\mathbf{D}\cdot\mathbf{S}\{S\}\,\frac{\mathrm{d}\Sigma(r)}{|\mathbf{n}|} = a^2 c\,r\oint \mathring{\mathbf{T}}\{T\}\cdot\mathring{\mathbf{S}}\{S\}\,\mathrm{d}\mathring{\Omega} = 0\,, \tag{2.9}$$

where $\mathbf{D} := \mathbf{L}\cdot\mathbf{L}$ is positive-definite. The $\mathbf{T}\{T\}$ and $\mathbf{S}\{S\}$ fields are orthogonal on $\Sigma(r)$ in the sense of the first integral. Also

$$\mathring{\mathbf{r}}\cdot\mathring{\mathbf{T}}\{T\} = 0\,,\quad \mathring{\mathbf{r}}\cdot\mathring{\mathbf{S}}\{S\} = -\mathring{\Lambda}^2 S\,,\quad \mathring{\nabla}\times\mathring{\mathbf{T}}\{T\} = \mathring{\mathbf{S}}\{T\}\,,\quad \mathring{\nabla}\times\mathring{\mathbf{S}}\{S\} = \mathring{\mathbf{T}}\{-\mathring{\nabla}^2 S\}\,. \tag{2.10}$$

Thus $\mathring{\nabla}\times\mathring{\mathbf{B}} = \mathring{\mathbf{T}}\{-\mathring{\nabla}^2 S\} + \mathring{\mathbf{S}}\{T\}$. It will be assumed throughout that any quantity in E^3 has a ringed version in $\mathring{E}^3$, except for r, θ, ϕ, the toroidal-poloidal potentials T, S, t, s, the basis vectors $\mathbf{1}_x$, $\mathbf{1}_y$, $\mathbf{1}_z$ and the derived quantity $Y_n^m(\theta,\phi)$.

2.2 The Spherically-Scaled Kinematic Dynamo Problem

It is shown in subsections (i)–(iii) that, if the coordinates and fields are scaled as in (2.4), the induction equation (1.1)(a) and (1.1)(c) are transformed using (2.6) to

$$\frac{\partial\mathring{\mathbf{B}}}{\partial\mathring{t}} = \left(\mathring{\nabla}^2 + \frac{e^2}{1-e^2}\partial_{\mathring{z}\mathring{z}}\right)\mathring{\mathbf{B}} + \mathring{R}_\mathrm{m}\mathring{\nabla}\times(\mathring{\mathbf{v}}\times\mathring{\mathbf{B}})\quad\text{in } \mathring{V};\quad \mathring{\nabla}\cdot\mathring{\mathbf{B}} = 0\quad\text{in } \mathring{E}^3, \tag{2.11}$$

where $\mathring{t} := t/a^2$ and $\mathring{R}_\mathrm{m} := a^2 R_\mathrm{m}$ are a scaled time and magnetic Reynolds number. Moreover, the current-free condition (1.1)(b) becomes

$$\mathring{\nabla}\times(\mathring{\mathbf{B}} - e^2\mathring{B}_z\mathbf{1}_z) = \mathbf{0}\,,\quad\text{in } \mathring{E}^3\setminus\mathring{V}. \tag{2.12}$$

The matching conditions at the boundary Σ and the self-exciting conditions as $r\to\infty$ (1.3) imply

$$[\mathring{\mathbf{B}}]_{\mathring{\Sigma}} = \mathbf{0}\,;\quad \mathring{\mathbf{B}} = \boldsymbol{\mathcal{O}}(r^{-3})\,,\quad\text{as } r\to\infty, \tag{2.13}$$

and conversely. Clearly $\mathbf{v}$ acts as a dynamo for the magnetic field $\mathbf{B}$, i.e. $\mathbf{B}$ grows, if and only $\mathring{\mathbf{v}}$ acts as a dynamo for $\mathring{\mathbf{B}}$; critical flows and magnetic fields correspond.

The mass conservation equation and velocity boundary condition (1.4) are transformed using (2.6) to

$$\frac{\partial\mathring{\rho}}{\partial\mathring{t}} + \mathring{R}_\mathrm{m}\mathring{\nabla}\cdot(\mathring{\rho}\mathring{\mathbf{v}}) = 0\,,\quad\text{in } \mathring{V};\quad \mathring{\mathbf{n}}\cdot\mathring{\mathbf{v}} = 0\quad\text{on } \mathring{\Sigma}; \tag{2.14}$$

defining $\mathring{\rho}$ by requiring $\int_{\delta\mathring{V}}\mathring{\rho}\,\mathrm{d}\mathring{V} = \int_{\delta V}\rho\,\mathrm{d}V$ for any corresponding volumes $\delta\mathring{V}$ and δV, i.e. $\mathring{\rho} = a^2 c\rho$. Hence the flow $\mathring{\mathbf{v}}$ is kinematically feasible if and only if $\mathbf{v}$ is kinematically feasible. In particular, $\mathring{\mathbf{v}}$ is incompressible if and only if $\mathbf{v}$ is incompressible; and $\mathring{\mathbf{n}}\cdot\mathring{\mathbf{v}} = 0$ on $\mathring{\Sigma}$ if and only if $\mathbf{n}\cdot\mathbf{v} = 0$ on Σ. The no-slip velocity condition is also preserved under (2.4), $\mathring{\mathbf{v}} = \mathbf{0}$ on $\mathring{\Sigma}$ if and only if $\mathbf{v} = \mathbf{0}$ on Σ, but the stress-free condition on $\mathbf{v}$ has a more complicated form for $\mathring{\mathbf{v}}$.

2.2.1 The Magnetic Induction Equation

By (2.6) (even without $\nabla \cdot \mathbf{B} = 0$),

$$\mathbf{L} \cdot \nabla \times (\mathbf{v} \times \mathbf{B}) = (\mathbf{L} \cdot \mathbf{v}) \nabla \cdot \mathbf{B} + \mathbf{B} \cdot \nabla (\mathbf{L} \cdot \mathbf{v}) - (\mathbf{L} \cdot \mathbf{B}) \nabla \cdot \mathbf{v} - \mathbf{v} \cdot \nabla (\mathbf{L} \cdot \mathbf{B}) = \mathring{\nabla} \times (\mathring{\mathbf{v}} \times \mathring{\mathbf{B}}) \,.$$

Thus in scaled coordinates the dot product of the magnetic induction equation (1.1)(a) with $\mathbf{L}$ yields

$$\partial_t \mathring{\mathbf{B}} = \mathring{\nabla} \cdot (\mathbf{D} \cdot \mathring{\nabla} \mathring{\mathbf{B}}) + R_{\mathrm{m}} \mathring{\nabla} \times (\mathring{\mathbf{v}} \times \mathring{\mathbf{B}}) \,, \tag{2.15}$$

where, using (2.5), the geometric diffusion tensor $\mathbf{D} := \mathbf{L} \cdot \mathbf{L}$ and its inverse can be written as

$$a^2 \mathbf{D} = \mathbf{I} + \frac{e^2}{1 - e^2} \mathbf{1}_z \mathbf{1}_z \,, \quad \mathbf{D}^{-1} = a^2 (\mathbf{I} - e^2 \mathbf{1}_z \mathbf{1}_z) \,. \tag{2.16}$$

Substituting (2.16) for $\mathbf{D}$ into (2.15) yields the spherically scaled magnetic induction equation (2.11)(a). The new feature of equation (2.11), over the magnetic induction equation (1.1), is the anisotropic geometric diffusion term which enhances the magnetic diffusion in the z-direction.

2.2.2 The Equations in the Insulating Exterior

The current-free condition (1.1)(b) in the insulating exterior $E^3 \setminus V$ transforms to

$$\nabla \times \mathbf{B} = \mathring{\nabla} \cdot \{ (\mathbf{L} \times \mathbf{L}^{-1}) \cdot \mathring{\mathbf{B}} \} = \mathbf{0} \,, \quad \text{in } \mathring{E}^3 \setminus \mathring{V}. \tag{2.17}$$

The equivalent but more useful equation (2.12) for the present formulation is derived here. Using the form (2.5) of $\mathbf{L}$,

$$\mathbf{B} = a(\mathring{\mathbf{B}} - f \mathring{B}_z \mathbf{1}_z) \,, \quad a \nabla = \mathring{\nabla} + \frac{f}{1 - f} \mathbf{1}_z \partial_{\mathring{z}} \,. \tag{2.18}$$

Substituting these two expressions directly into (1.1)(b) gives

$$\nabla \times \mathbf{B} = \mathring{\nabla} \times \mathring{\mathbf{B}} - f \mathring{\nabla} \times \mathring{B}_z \mathbf{1}_z + \frac{f}{1 - f} \mathbf{1}_z \times \partial_{\mathring{z}} \mathring{\mathbf{B}} = \mathbf{0} \,, \quad \text{in } \mathring{E}^3 \setminus \mathring{V}. \tag{2.19}$$

It is not obvious that the vector equation (2.19) is equivalent to two scalar equations in T and S. However, observe that (2.19) implies

$$\mathbf{1}_z \cdot \mathring{\nabla} \times \mathring{\mathbf{B}} = 0 \quad \text{in } \mathring{E}^3 \setminus \mathring{V}. \tag{2.20}$$

The $\mathring{\nabla}$-divergence of the middle expression in (2.19) gives $\partial_{\mathring{z}} (\mathbf{1}_z \cdot \mathring{\nabla} \times \mathring{\mathbf{B}})$, which vanishes identically if (2.20) is satisfied, so that (2.19) is in fact equivalent to just two scalar equations. This can be seen more clearly by contracting the left equation in (2.19) with $\mathbf{L}$, which yields

$$a \mathbf{L} \cdot \nabla \times \mathbf{B} = \mathring{\nabla} \times \mathring{\mathbf{B}} - f \mathring{\nabla} \times \mathring{B}_z \mathbf{1}_z + \frac{f}{1 - f} (\mathbf{1}_z \times \partial_{\mathring{z}} \mathring{\mathbf{B}} + \mathbf{1}_z \mathbf{1}_z \cdot \mathring{\nabla} \times \mathring{\mathbf{B}}) \,. \tag{2.21}$$

Using the identity $\mathring{\nabla} \times \mathring{B}_z \mathbf{1}_z + \mathbf{1}_z \times \partial_{\mathring{z}} \mathring{\mathbf{B}} + \mathbf{1}_z \mathbf{1}_z \cdot \mathring{\nabla} \times \mathring{\mathbf{B}} = \mathring{\nabla} \times \mathring{\mathbf{B}}$ and $2f - f^2 = e^2$ reduces (2.21) to

$$a(1 - f) \mathbf{L} \cdot \nabla \times \mathbf{B} = \mathring{\nabla} \times (\mathring{\mathbf{B}} - e^2 \mathring{B}_z \mathbf{1}_z) \,. \tag{2.22}$$

Thus the current-free conditions (1.1)(b), (2.17) or (2.19) are equivalent to the current-free condition (2.12). This equation differs in form from the original current-free condition (1.1)(b) by a subtractive $\mathcal{O}(e^2)$ geometric anisotropy $e^2 \mathring{\nabla} \times \mathring{B}_z \mathbf{1}_z$.

By (1.1)(b) there exists a magnetic scalar potential Ψ with $\mathbf{B} = -\nabla \Psi$ in $E^3 \setminus V$ and $\nabla^2 \Psi = 0$ by (1.1)(c). The potential Ψ and $\mathring{\mathbf{B}}$ are related by $\mathring{\mathbf{B}} = -\mathbf{D} \cdot \mathring{\nabla} \Psi$ where $\mathbf{D}$ is given by (2.16) and since $\nabla^2 = \mathring{\nabla} \cdot \mathbf{D} \cdot \mathring{\nabla}$, Ψ satisfies the elliptic equation $\mathring{\nabla} \cdot \mathbf{D} \cdot \mathring{\nabla} \Psi = 0$. Hence

$$\mathring{\mathbf{B}} = -\Big(\mathring{\nabla} + \frac{e^2}{1 - e^2} \mathbf{1}_z \partial_{\mathring{z}} \Big) \Psi / a^2 \,, \quad \Big(\mathring{\nabla}^2 + \frac{e^2}{1 - e^2} \partial_{\mathring{z}} \partial_{\mathring{z}} \Big) \Psi = 0 \,, \quad \text{in } \mathring{E}^3 \setminus \mathring{V}.$$

In cylindrical polar coordinates, $\mathring{B}_s = -\partial_{\mathring{s}} \Psi / a^2$, $\mathring{B}_\phi = -\mathring{s}^{-1} \partial_\phi \Psi / a^2$, $\mathring{B}_z = -\partial_{\mathring{z}} \Psi / c^2$. The equation $\nabla^2 \Psi = 0$ implies $\nabla^2 (\nabla \Psi)^2 = 2 \nabla \nabla \Psi : \nabla \nabla \Psi \geq 0$ and $(\mathring{\nabla} \cdot \mathbf{D} \cdot \mathring{\nabla})(\mathring{\nabla} \Psi)^2 = 2 \operatorname{tr}[(\mathring{\nabla} \mathring{\nabla} \Psi)^T \cdot \mathbf{D} \cdot \mathring{\nabla} \mathring{\nabla} \Psi] \geq 0$. Thus the elliptic interior maximum principle (Protter and Weinberger, 1984) implies, noting (1.3)(c), that $\max_{E^3 \setminus V} |\mathbf{B}|$ occurs on Σ and $\max_{\mathring{E}^3 \setminus \mathring{V}} |\mathring{\mathbf{B}}|$ on $\mathring{\Sigma}$, although not necessarily at corresponding points.

2.2.3 The Toroidal and Poloidal Equations

The solenoidal condition (2.11)(b) is satisfied by the toroidal-poloidal representation (2.7). Equations for the toroidal-poloidal potentials T and S in $\mathring{V}$ follow from (2.11)(a) by using (2.10),

$$(\partial_{\mathring{t}} - \mathring{\nabla}^2)\mathring{\Lambda}^2 S = -\frac{e^2}{1-e^2}\mathring{\mathbf{r}}\cdot\partial_{\mathring{z}\mathring{z}}\mathring{\mathbf{B}} - \mathring{R}_{\rm m}\mathring{\mathbf{r}}\cdot\mathring{\nabla}\times(\mathring{\mathbf{v}}\times\mathring{\mathbf{B}}) \tag{2.23}$$

$$(\partial_{\mathring{t}} - \mathring{\nabla}^2)\mathring{\Lambda}^2 T = -\frac{e^2}{1-e^2}\mathring{\mathbf{r}}\cdot\mathring{\nabla}\times\partial_{\mathring{z}\mathring{z}}\mathring{\mathbf{B}} - \mathring{R}_{\rm m}\mathring{\mathbf{r}}\cdot\mathring{\nabla}\times\mathring{\nabla}\times(\mathring{\mathbf{v}}\times\mathring{\mathbf{B}})\,. \tag{2.24}$$

In $\mathring{E}^3\setminus\mathring{V}$, since the $\mathring{\nabla}$-divergence of the left side of (2.12) is zero, the properties (2.10) of toroidal-poloidal fields imply (2.12) is equivalent to the two scalar equations

$$\mathring{\mathbf{r}}\cdot\mathring{\nabla}\times(\mathring{\mathbf{B}} - e^2\mathring{B}_z\mathbf{1}_z) = 0\,, \quad \mathring{\mathbf{r}}\cdot\mathring{\nabla}\times\mathring{\nabla}\times(\mathring{\mathbf{B}} - e^2\mathring{B}_z\mathbf{1}_z) = 0\,. \tag{2.25}$$

Expressions in T and S follow from the identities $\mathbf{r}\cdot\nabla\times f\mathbf{1}_z = \partial_\phi f$, (2.10), $\mathring{\mathbf{r}}\cdot\mathring{\nabla}\times\mathring{\nabla}\times(f\mathbf{1}_z) = r\partial_r\partial_{\mathring{z}} f - r\cos\theta\,\mathring{\nabla}^2 f$, $\mathbf{1}_z = \cos\theta\mathbf{1}_r - \sin\theta\mathbf{1}_\theta$ and $\partial_{\mathring{z}} = \cos\theta\,\partial_r - r^{-1}\sin\theta\,\partial_\theta$. Thus

$$\mathring{B}_z = \mathring{B}_r\cos\theta - \mathring{B}_\theta\sin\theta = -\frac{\cos\theta}{r}\mathring{\Lambda}^2 S - \frac{\sin\theta}{r}\partial_\theta\partial_r(rS) - \partial_\phi T\,, \tag{2.26}$$

and the left sides of (2.25) become

$$\mathring{\mathbf{r}}\cdot\mathring{\nabla}\times(\mathring{\mathbf{B}} - e^2\mathring{B}_z\mathbf{1}_z) = -\mathring{\Lambda}^2 T + e^2\Big(\frac{\cos\theta}{r}\mathring{\Lambda}^2\partial_\phi S + \frac{\sin\theta}{r}\partial_\theta\partial_r(r\partial_\phi S) + \partial_{\phi\phi}T\Big) \tag{2.27}$$

$$\begin{aligned}\mathring{\mathbf{r}}\cdot\mathring{\nabla}\times\mathring{\nabla}\times(\mathring{\mathbf{B}} - e^2\mathring{B}_z\mathbf{1}_z) = {}& \mathring{\Lambda}^2\mathring{\nabla}^2 S + e^2\{r\partial_r(\cos\theta\,\partial_r - \sin\theta\,\partial_\theta) - r\cos\theta\,\mathring{\nabla}^2\}\\ & + \Big(\frac{\cos\theta}{r}\mathring{\Lambda}^2 S + \frac{\sin\theta}{r}\partial_\theta\partial_r(rS) + \partial_\phi T\Big)\,.\end{aligned} \tag{2.28}$$

From properties of the operator $\mathring{\Lambda}^2$, (2.25) with (2.27) and (2.28) reduce to the spherical equations $T = 0$ and $\mathring{\nabla}^2 S = 0$ in the limit $e \to 0$. In general, if $e > 0$ they couple non-axisymmetric T and S fields in $r > 1$. Equations different from (2.25) are possible, e.g. for $e > 0$ equations (2.20) and (2.26), noting (2.10), imply

$$\frac{\cos\theta}{r}\mathring{\Lambda}^2 T + \frac{\sin\theta}{r}\partial_\theta\partial_r(rT) - \mathring{\nabla}^2\partial_\phi S = 0\,, \quad \text{in } \mathring{E}^3\setminus\mathring{V}. \tag{2.29}$$

By (2.27) and (2.28), conditions (2.3) and (2.25) are equivalent to conditions (1.1)(b) and (1.3). However, it is not obvious that conditions (2.3) together with (2.12) are sufficient to guarantee that no current crosses Σ. Observe that the dot product of (2.12) with $\mathring{\mathbf{r}}$ yields $a(1-f)\mathbf{n}\cdot\nabla\times\mathbf{B} = \mathring{\mathbf{r}}\cdot\mathring{\nabla}\times(\mathring{\mathbf{B}} - e^2\mathring{B}_z\mathbf{1}_z)$, since $\mathbf{n} = \mathbf{L}\cdot\mathring{\mathbf{r}}$. Apart from factors $a(1-f)|\mathbf{n}|$ and $|\mathring{\mathbf{r}}|$ the expressions on the left and first on the right are the normal components of the (dimensionless) current on Σ and $\mathring{\Sigma}$. The difficulty is the $\mathring{B}_z$ term. From (2.3) and (2.27), $[\mathring{\mathbf{r}}\cdot\mathring{\nabla}\times(\mathring{\mathbf{B}} - e^2\mathring{B}_z\mathbf{1}_z)]_{\mathring{\Sigma}} = 0$. Hence $[\mathbf{n}\cdot\nabla\times\mathbf{B}]_\Sigma = 0$ and thus $\mathbf{n}\cdot\nabla\times\mathbf{B} = 0$ on Σ^-.

Finally, if $\mathring{\mathbf{v}}$ (equivalently $\mathbf{v}$) satisfies the impenetrable boundary condition (2.14)(b) the velocity poloidal scalar s satisfies

$$s = 0 \quad \text{at } r = 1. \tag{2.30}$$

3 Numerical Method

Equations (2.11), (2.12) and (2.13) are solved by discretising the toroidal-poloidal equations (2.23), (2.24), (2.25) with (2.27) and (2.28), using a Galerkin method in angle with spherical harmonics as the basis functions and second-order finite differences in radius for simplicity, and solving subject to (2.3). Other radial discretisation methods are possible.

3.1 The Angular Spectral Equations

The magnetic toroidal-poloidal potentials are expanded in spherical harmonics,

$$f = \sum_{n,m} f_n^m(r,\mathring{t})Y_n^m(\theta,\phi)\,, \quad Y_n^m(\theta,\phi) := (-)^m\sqrt{\frac{(2n+1)(n-m)!}{(n+m)!}}P_{n,m}(\cos\theta)e^{im\phi}\,, \tag{3.1}$$

where $f = T$ or S, and $P_{n,m}$ is the Neumann associated Legendre function,

$$P_{n,m}(z) := (1-z^2)^{m/2}\frac{\mathrm{d}^m P_n(z)}{\mathrm{d}z^m}\,, \quad P_n(z) = \frac{1}{2^n n!}\frac{\mathrm{d}^n}{\mathrm{d}z^n}(z^2-1)^n\,. \tag{3.2}$$

Also $(Y_n^m)^* = (-)^m Y_n^{-m}$ where an asterisk denotes complex conjugation; $\mathring{\Lambda}^2 Y_n^m = -\lambda_n Y_n^m$ where $\lambda_n := n(n+1)$; and $\mathring{\nabla}^2 f(r) Y_n^m = \mathrm{D}_n f(r) Y_n^m$ for any function $f(r)$, where $\mathrm{D}_n := r^{-2}[\partial_r(r^2\partial_r) - \lambda_n]$. The spherical harmonics (3.1) form a complete orthonormal set with respect to the inner-product $(f,g) := \oint fg^*\,\mathrm{d}\mathring{\Omega}/4\pi$ of complex scalar functions f and g on $\mathring{\Sigma}(r)$. The $n=0$ terms do not contribute to the vector fields and are omitted. The boundary, matching and self-exciting conditions (2.3) imply the spherical harmonic coefficients satisfy

$$[S_n^m]_{r=1} = 0\,,\ [\partial_r S_n^m]_{r=1} = 0\,,\ [T_n^m]_{r=1} = 0\,; \quad S_n^m = \mathcal{O}(r^{-2})\,,\ T_n^m = \mathcal{O}(r^{-3}) \quad \text{as } r\to\infty. \tag{3.3}$$

For a self-exciting insulated spherical dynamo the behaviour of T as $r\to\infty$ does not arise as in (3.3) since T then vanishes in $E^3 \setminus V$.

3.1.1 The Conducting Region

The spectral forms of the poloidal and toroidal induction equations (2.23) and (2.24) are

$$(\partial_{\mathring{t}} - \mathrm{D}_n)S_n^m = \frac{e^2}{1-e^2}\mathcal{S}_n^m\{\partial_{\mathring{z}\mathring{z}}\mathring{\mathbf{B}}\} + R_\mathrm{m}\mathcal{S}_n^m\{\mathring{\nabla}\times(\mathring{\mathbf{v}}\times\mathring{\mathbf{B}})\} \tag{3.4}$$

$$(\partial_{\mathring{t}} - \mathrm{D}_n)T_n^m = \frac{e^2}{1-e^2}\mathcal{T}_n^m\{\partial_{\mathring{z}\mathring{z}}\mathring{\mathbf{B}}\} + R_\mathrm{m}\mathcal{T}_n^m\{\mathring{\nabla}\times(\mathring{\mathbf{v}}\times\mathring{\mathbf{B}})\}\,, \tag{3.5}$$

where the (reduced) poloidal transform and the toroidal transform are defined by

$$\mathcal{S}_n^m\{\mathbf{F}\} := \frac{1}{4\pi\lambda_n}\oint Y_n^{m*}\mathbf{r}\cdot\mathbf{F}\,\mathrm{d}\mathring{\Omega}\,, \quad \mathcal{T}_n^m\{\mathbf{F}\} := \frac{1}{4\pi\lambda_n}\oint Y_n^{m*}\boldsymbol{\Lambda}\cdot\mathbf{F}\,\mathrm{d}\mathring{\Omega}\,. \tag{3.6}$$

The horizontal divergence equation is redundant as shown in Appendix A.

In time-stepping problems, the transforms (3.6) of the induction term are most efficiently calculated numerically from values of $\mathbf{F}$ on a (θ,ϕ)-grid using fast-Fourier transforms in ϕ and Gaussian quadrature in θ. However, in the eigen- and critical-value problems for steady flows considered here the transforms are evaluated using angular spectral expansions (Bullard and Gellman, 1954, Elsasser, 1946); see Appendix B. The transforms of the anisotropic diffusion terms are more problematic. The angular spectral forms of the anisotropic magnetic diffusion terms in (3.4) and (3.5) have relatively few terms, and so are preferable here to the numerical calculation of (3.6). The transforms are

$$\mathcal{S}_n^m\{\partial_{\mathring{z}\mathring{z}}\mathring{\mathbf{B}}\} = L_n^m(S,T)\,, \qquad \mathcal{T}_n^m\{\partial_{\mathring{z}\mathring{z}}\mathring{\mathbf{B}}\} = L_n^m(T,-\mathring{\nabla}^2 S)\,. \tag{3.7}$$

where the differential operator L_n^m is defined by

$$L_n^m(F,G) := \frac{n-2}{n}c_{n-1,n}^m \mathrm{D}_{1-n,2-n}F_{n-2}^m + \frac{2imc_n^m}{n(n+1)}\mathrm{d}_{1-n}G_{n-1}^m + C_n^m\mathrm{D}_n F_n^m + \frac{2imc_{n+1}^m}{n(n+1)}\mathrm{d}_{n+2}G_{n+1}^m + \frac{n+3}{n+1}c_{n+1,n+2}^m\mathrm{D}_{n+2,n+3}F_{n+2}^m\,, \tag{3.8}$$

and the operators $\mathrm{d}_n := \partial_r + n/r$ and $\mathrm{D}_{n_1,n_2} := \mathrm{d}_{n_1}\mathrm{d}_{n_2}$. The coefficients are defined by $c_n^m := \sqrt{(n^2-m^2)/(4n^2-1)}$, $c_{n_1,n_2}^m := c_{n_1}^m c_{n_2}^m$ and

$$C_n^m := \frac{n-2}{n}c_{n,n}^m + \frac{n+3}{n+1}c_{n+1,n+1}^m\,. \tag{3.9}$$

Expansions (3.8) may be derived using the recurrence relations

$$\cos\theta\ Y_n^m = c_{n+1}^m\ Y_{n+1}^m + c_n^m\ Y_{n-1}^m\,, \quad \sin\theta\ \partial_\theta Y_n^m = nc_{n+1}^m\ Y_{n+1}^m - (n+1)c_n^m\ Y_{n-1}^m\,. \tag{3.10}$$

The poloidal and toroidal equations (3.4) and (3.5) hold for $n=1$ and $n=2$, since the factor c_n^m in the first two terms of (3.8) vanishes for $n=1$ (forcing $m=1$) and the first term clearly vanishes for $n=2$. The right side of equation (3.7)(b) contains third-order radial derivatives of S_n^m through the terms $\mathrm{d}_{1-n}\mathrm{D}_{n-1}S_{n-1}^m$ and $\mathrm{d}_{n+2}\mathrm{D}_{n+1}S_{n+1}^m$ but only second-order derivatives of T_n^m.

3.1.2 The Insulating Exterior

The angular spectral forms of the exterior equations (2.25) with (2.27) and (2.28) are now derived. Each term is treated separately. The expansions of the first terms are $\mathring{\mathbf{r}}\cdot\mathring{\nabla}\times\mathring{\mathbf{B}} = -\mathring{\Lambda}^2 T = \sum_{n,m}\lambda_n T_n^m Y_n^m$ and $\mathring{\mathbf{r}}\cdot\mathring{\nabla}\times(\mathring{\nabla}\times\mathring{\mathbf{B}}) = \mathring{\Lambda}^2\mathring{\nabla}^2 S = -\sum_{n,m}\lambda_n D_n S_n^m Y_n^m$. The expansions of the second term in each equation follow from $\mathbf{r}\cdot\nabla\times f\mathbf{1}_z = \partial_\phi f = \sum_{n,m} im f_n^m Y_n^m$,

$$\mathring{\mathbf{r}}\cdot\mathring{\nabla}\times\mathring{\nabla}\times(f\mathbf{1}_z) = \nabla\cdot[(\mathring{\nabla}f\times\mathbf{1}_z)\times\mathring{\mathbf{r}}] = \nabla\cdot(r\partial_r f\mathbf{1}_z - r\cos\theta\mathring{\nabla}f) = r\partial_r\partial_{\mathring{z}} f - r\cos\theta\,\mathring{\nabla}^2 f$$

and the formulae

$$\mathbf{r}\cdot\nabla\times\nabla\times(f\mathbf{1}_z) = \sum_{n,m}\left\{-(n+1)c_n^m d_{1-n} f_{n-1}^m + n c_{n+1}^m d_{n+2} f_{n+1}^m\right\} Y_n^m\,,$$

$$\mathring{B}_z = \sum_{n,m}\left\{-(n-1)c_n^m d_{1-n} S_{n-1}^m - im T_n^m + (n+2)c_{n+1}^m d_{n+2} S_{n+1}^m\right\} Y_n^m\,, \tag{3.11}$$

which can be derived using relations (3.10). Thus the spectral forms of (2.27) and (2.28) give

$$\lambda_n T_n^m - e^2\Big\{ - im(n-1)c_n^m \mathrm{d}_{1-n} S_{n-1}^m + m^2 T_n^m + im(n+2)c_{n+1}^m \mathrm{d}_{n+2} S_{n+1}^m\Big\} = 0 \tag{3.12}$$

$$\begin{aligned}\mathrm{D}_n S_n^m + e^2\Big\{ &\frac{n-2}{n} c_{n-1,n}^m \mathrm{D}_{1-n,2-n} S_{n-2}^m + \frac{imc_n^m}{n}\mathrm{d}_{1-n} T_{n-1}^m - \widehat{C}_n^m \mathrm{D}_n S_n^m \\ &- \frac{imc_{n+1}^m}{n+1}\mathrm{d}_{n+2} T_{n+1}^m + \frac{n+3}{n+1} c_{n+1,n+2}^m \mathrm{D}_{n+2,n+3} S_{n+2}^m\Big\} = 0\,.\end{aligned} \tag{3.13}$$

where

$$\widehat{C}_n^m := \frac{n+1}{n} c_{n,n}^m + \frac{n}{n+1} c_{n+1,n+1}^m\,. \tag{3.14}$$

3.2 Radial Discretisation

The radial dependence is discretised using second-order finite differences. In the interior $0 \le r \le 1-$ a uniform radial grid is used: $r_j = jh$, $j = 0:J$, with step size $h = 1/J$ and $r_J = 1-$. In the exterior $1+ \le r < \infty$ a uniform grid in the inverse radial coordinate $\xi = 1/r$ is used: $\xi_j = 1 + jh_\xi$, $j = 0:J_\xi$, with step size $h_\xi = -1/J_\xi$. Additional interior and exterior limiting grid points $r = 1-$ and $r = 1+$ are allocated to the boundary $r = 1$ to simplify implementation of the finite-differencing. Thus the full radial grid is $r_j = jh$ for $j = 0:J$ and $r_j = 1/[1 + (j-J)h_\xi]/$ for $j = J{+}1 : J{+}J_\xi$ with $r_J = 1-$, $r_{J+1} = 1$ and $r_{J+2} = 1+$. See table 1. The truncation levels J, J_ξ and the related step sizes h, h_ξ can be specified independently.

The S_n^m and T_n^m equations (3.4) and (3.5) are discretised at internal radial grid points in $\mathring{V}$; the S_n^m equation is also discretised at the boundary grid point $r = 1-$. The T_n^m equation is not discretised at $r = 1-$, since T_n^m is continuous across the boundary by (3.3) but $\partial_r T_n^m$ may be discontinuous. The S_n^m and T_n^m equations (3.12) and (3.13) are discretised at the grid points in the exterior $E^3 \setminus V$. There is one equation for each of the coefficient values $T_n^m(r_j)$ and $S_n^m(r_j)$ at each grid-point r_j. Matching conditions are applied as shown in table 1.

3.2.1 The Conducting Interior

The following one-sided second-order right-boundary schemes are used at or near the boundary.

$$f_0^{(1)} = \tfrac{1}{2}h^{-1}(f_{-2} - 4f_{-1} + 3f_0) + \tfrac{1}{3}f^{(3)}(\eta)h^2 \tag{3.15}$$

$$f_0^{(2)} = h^{-2}(-f_{-3} + 4f_{-2} - 5f_{-1} + 2f_0) + \tfrac{11}{12}f^{(4)}(\eta)h^2 \tag{3.16}$$

$$f_0^{(2)} = \tfrac{1}{2}h^{-2}\Big(- f_{-2} + 8f_{-1} - 7f_0 + 6hf_0^{(1)}\Big) + \tfrac{1}{6}f^{(4)}(\eta)h^2 \tag{3.17}$$

$$f_0^{(3)} = h^{-3}\Big(f_{-3} - 6f_{-2} + 15f_{-1} - 10f_0 + 6hf_0^{(1)}\Big) + \tfrac{11}{20}f^{(5)}(\eta)h^2 \tag{3.18}$$

$$f_0^{(3)} = \tfrac{1}{3}h^{-3}\Big(- f_{-2} + 9f_0 - 8f_1 + 6hf_1^{(1)}\Big) - \tfrac{3}{20}f^{(5)}(\eta)h^2\,. \tag{3.19}$$

Schemes (3.15) and (3.16) are used for the T field at r_J; schemes (3.17)–(3.19), which include the first derivative at the boundary, are used for the second and third derivatives of the S field at r_J or r_{J-1}. Otherwise centred formulas are used for the T and S fields.

Radial Block	Radius	Equations	Fields
1	h	S_n^m de, T_n^m de	S_n^m, T_n^m
$\vdots$	$\vdots$	$\vdots$	$\vdots$
$J-1$	$1-h=(J-1)h$	S_n^m de, T_n^m de	S_n^m, T_n^m
J	$1-=Jh$	S_n^m de, T_n^m mc	S_n^m, T_n^m
$J+1$	1	S_n^m mc	$\partial_r S_n^m$
$J+2$	$1+=(1+0h_\xi)^{-1}$	S_n^m de, T_n^m de	S_n^m, T_n^m
$J+3$	$(1+h_\xi)^{-1}$	S_n^m de, T_n^m de	S_n^m, T_n^m
$\vdots$	$\vdots$	$\vdots$	$\vdots$
$J+J_\xi+1$	$(1+(J_\xi-1)h_\xi)^{-1}$	S_n^m de, T_n^m de	S_n^m, T_n^m

Table 1: The ordering of differential equations (de) and matching conditions (mc) for S_n^m and T_n^m into radial blocks. Note $h_\xi < 0$.

3.2.2 Insulating Exterior

The change of variable from r to ξ in equations (3.12) and (3.13) is accomplished with the identities, $r\partial_r = -\xi\partial_\xi$, $\partial_r = -\xi^2\partial_\xi$. Define the operators $\mathrm{d}_a^\xi := \partial_\xi + a\xi^{-1}$, $\mathrm{D}_{a,b}^\xi := \mathrm{d}_a^\xi \mathrm{d}_b^\xi$ and $\mathrm{D}_n^\xi := \partial_{\xi\xi} - \lambda_n\xi^{-2}$, where a, b are constants. Then $\mathrm{d}_a = -\xi^2\mathrm{d}_{-a}^\xi$, $\mathrm{D}_{a,b} = \xi^4\mathrm{D}_{2-a,-b}^\xi$, $\mathrm{D}_n^\xi = \mathrm{D}_{-n,n}^\xi$ and $\mathrm{D}_n = \mathrm{D}_{n+2,-n} = \xi^4\mathrm{D}_{-n,n}^\xi = \xi^4\mathrm{D}_n^\xi$. Thus the toroidal and poloidal equations become

$$\lambda_n T_n^m + e^2\{-im(n-1)c_n^m\xi^2\mathrm{d}_{n-1}^\xi S_{n-1}^m + im(n+2)c_{n+1}^m\xi^2\mathrm{d}_{-n-2}^\xi S_{n+1}^m - m^2 T_n^m\} = 0 \tag{3.20}$$

$$\begin{aligned}\xi^2 D_n^\xi S_n^m + e^2\Bigg\{ &\frac{n-2}{n}c_{n-1,n}^m\xi^2\mathrm{D}_{n+1,n-2}^\xi S_{n-2}^m - \frac{im}{n}c_n^m\mathrm{d}_{n-1}^\xi T_{n-1}^m - \widehat{C}_n^m\xi^2\mathrm{D}_n^\xi S_n^m \\ &+\frac{im}{n+1}c_{n+1}^m\mathrm{d}_{-n-2}^\xi T_{n+1}^m + \frac{n+3}{n+1}c_{n+1,n+2}^m\xi^2\mathrm{D}_{-n,-n-3}^\xi S_{n+2}^m\Bigg\} = 0\,.\end{aligned} \tag{3.21}$$

The left boundary difference schemes used in the exterior are obtained by replacing h by $-h$ in the corresponding right schemes and used in the S-equation (3.21) at r_{J+2} for the T and S fields.

3.3 Eigen- and Critical-Value Problems for Steady Flows

For steady flows magnetic field solutions can be found with time dependence $\mathring{\mathbf{B}} \propto e^{\mathring{\gamma}\,\mathring{t}} = e^{\gamma t}$, where t is the time and the growth rates are related by $\mathring{\gamma} = a^2\gamma$. Growth, criticality and decay are preserved by the scaling: $\mathrm{Re}\,\mathring{\gamma} = \mathrm{Re}\,\gamma = 0$ or $\mathrm{Re}\,\mathring{\gamma}\,\mathrm{Re}\,\gamma > 0$. Computations use $\mathring{\gamma}$ and the magnetic Reynolds number $\mathring{R}_\mathrm{m} = a^2 R_\mathrm{m}$, and the shape parameter a/c (or c/a) is prescribed. Values of the growth rates and magnetic Reynolds numbers for different length scales can be derived from computations by scaling with the shape parameter. Since the growth rate $\mathring{\gamma}$ depends only on the shape and $\mathring{R}_\mathrm{m}$, $\gamma(a,c,R_\mathrm{m}) = a^{-2}\mathring{\gamma}(c/a,\mathring{R}_\mathrm{m})$. Thus, if the length scale $\mathcal{L}$ is the major or minor semi-axis, spherical radius or circle radius, so that $a=1$, $c=1$, $a^2c=1$ or $ac=1$, the associated growth rates γ and magnetic Reynolds numbers R_m are given by $\mathring{\gamma}$, $\mathring{\gamma}(c/a)^2$, $\mathring{\gamma}(c/a)^{2/3}$ or $\mathring{\gamma}(c/a)$, and $\mathring{R}_\mathrm{m}$, $\mathring{R}_\mathrm{m}(c/a)^2$, $\mathring{R}_\mathrm{m}(c/a)^{2/3}$ or $\mathring{R}_\mathrm{m}(c/a)$, respectively. Setting $a=1$ gives $\mathring{\gamma}(c,R_\mathrm{m}) = \gamma(1,c,R_\mathrm{m})$, and hence $\gamma(a,c,R_\mathrm{m}) = a^{-2}\gamma(1,c/a,a^2R_\mathrm{m})$.

The spatial discretisation approximates the problem by a matrix generalised eigenproblem $\mathbf{A}\mathbf{x} = \mathring{\gamma}\mathbf{B}\mathbf{x}$, where the matrix $\mathbf{B}$ is singular. The discretisation produces banded matrices with the narrowest band, in general, if all coefficients and their equations at each grid point are blocked together. The matrix $\mathbf{A}$ is essentially block-pentadiagonal due to the centred difference formulas with the one-sided formulas (3.16), (3.17) and (3.19) distorting this slightly. In principle the generalised eigenvalues $\mathring{\gamma}$ are the zeros of the characteristic polynomial $\det(\mathring{\gamma}\mathbf{B} - \mathbf{A}) = 0$. If the matrices $\mathbf{A}$ and $\mathbf{B}$ are $N\times N$, the leading coefficient of this polynomial is $\det\mathbf{B}$, which is zero since $\mathbf{B}$ is singular. Accordingly there are less than N generalised eigenvalues. In fact, generally there may be $0, 1, \ldots, N-1$, or infinitely-many eigenvalues if the characteristic polynomial vanishes identically. Thus the generalised problems with $\mathbf{A} = \mathbf{A}_1$, $\mathbf{A}_0$ or $\mathbf{A}_\infty$ and $\mathbf{B}$, where

$$\mathbf{A}_1 := \begin{pmatrix}-1 & 0\\ 0 & 1\end{pmatrix}; \quad \mathbf{A}_0 := \begin{pmatrix}1 & 0\\ 1 & 1\end{pmatrix}; \quad \mathbf{A}_\infty := \begin{pmatrix}0 & 0\\ 1 & 1\end{pmatrix}; \quad \mathbf{B} := \begin{pmatrix}1 & 1\\ 0 & 0\end{pmatrix};$$

have one ($\gamma = -1$), zero and ∞-many eigensolutions. Despite this theoretical aspect of the generalised eigenproblem no difficulty, such as phantom eigenvalues, which may occur with the QZ-algorithm, has been

observed in practice with the methods used to determine selected generalised eigenvalues of the kinematic dynamo problem: inverse iteration, the implicitly restarted Arnoldi method and the power method with the conformal transformation $w = -(z-z_1)/(z-z_2)$. The transformation maps the half-plane $\mathrm{Re}\, z > 0$ to the exterior of the circle $|w| = 1$, $z_1 \mapsto 0$, $z_2 \mapsto \infty$ and $\frac{1}{2}(z_1+z_2) \mapsto 1$. The line $\mathrm{Re}\, z = c$ is mapped to the circle

$$(c-z_2)w\overline{w} + [c - \tfrac{1}{2}(z_1+z_2)](w+\overline{w}) + c - z_1 = 0\,,$$

with centre $[c - \frac{1}{2}(z_1+z_2)]/(c-z_2)$ and radius $\frac{1}{2}|z_1-z_2|/|c-z_2|$. Applying this mapping to the spectrum of the generalised eigenproblem yields a method for finding the eigenvalue of largest real part: apply the power method to the matrix $\mathbf{M} := -\mathbf{I} - (z_2-z_1)(\mathbf{A}-z_2\mathbf{B})^{-1}\mathbf{B}$.

3.4 Magnetic Energy and Related Seminorms

Norms and seminorms can be useful to estimate numerical convergence (Bachtiar and James, 2010). Useful spheroidal seminorms of a scalar field f on E^3 are defined by

$$|f|_{2,r}^2 := \frac{1}{4\pi}\oint_{\mathring{\Sigma}(r)} f^2\, \mathrm{d}\mathring{\Omega}\,, \quad \|f\|_{2,G}^2 := \frac{1}{4\pi}\int_G f^2\, \mathrm{d}\mathring{V}\,,$$

where the first integral is taken over a spheroidal r-surface and G is a region in $\mathring{E}^3$. The seminorm $|f|_{2,E^3}$ is a norm, i.e. it is zero only if $f = 0$ in E^3, which is denoted $\|f\|_2 := \|f\|_{2,E^3}$. The subscript 2's are suppressed below. The squared norm can be split into internal and external parts: $\|f\|^2 = \|f\|_V^2 + \|f\|_{E^3\setminus V}^2$. Also

$$\|f\|^2 = \int_0^\infty |f|_r^2\, r^2 dr\,, \quad \|f|_V^2 = \int_0^1 |f|_r^2\, r^2 dr\,, \quad |f|_{E^3\setminus V}^2 = \int_0^1 |f|_{\xi^{-1}}^2\, \xi^{-4} d\xi\,.$$

Related seminorms of a vector field $\mathbf{F}$ on E^3 are obtained by setting $f = F := |\mathbf{F}|$; thus $|\mathbf{F}|_r := |F|_r$ and $\|\mathbf{F}\|_G := \|F\|_G$.

A weighted magnetic energy on $\Sigma(r)$ is $2\pi a^2 E(r)$, where

$$E(r) := |\mathbf{B}/a|_r^2 = \frac{1}{4\pi}\oint (\mathring{\mathbf{B}}^2 - e^2\mathring{B}_z^2)\, d\mathring{\Omega} = \int_{\Sigma(r)} \tfrac{1}{2}\mathbf{B}^2 |2\pi a^4 c r\mathbf{n}|^{-1}\, d\Sigma\,.$$

Since any $\mathring{\mathbf{T}}$ and $\mathring{\mathbf{S}}$ are orthogonal over any $\mathring{\Sigma}(r)$ by (2.9) and $2f - f^2 = e^2$,

$$E(r) = |\mathring{\mathbf{T}}|_r^2 + |\mathring{\mathbf{S}}|_r^2 - e^2|\mathring{B}_z|_r^2\,. \tag{3.22}$$

The total magnetic energy in E^3 is $2\pi a^4 c E_B$, where

$$E_B := \|\mathbf{B}/a\|^2 = \|\mathring{\mathbf{T}}\|^2 + \|\mathring{\mathbf{S}}\|^2 - e^2\|\mathring{B}_z\|^2 = \int_0^\infty E(r) r^2\, \mathrm{d}r\,. \tag{3.23}$$

In spherical harmonic spectral form, $|\mathring{\mathbf{T}}|_r^2 = \sum_{n,m} \lambda_n |T_n^m|^2$, $r^2|\mathring{\mathbf{S}}|_r^2 = \sum_{n,m}\{\lambda_n^2|S_n^m|^2 + \lambda_n|\partial_r(rS_n^m)|^2\}$ and from (3.11),

$$r^2|\mathring{B}_z|_r^2 = \sum_{n,m} \left|-(n-1)c_n^m\,[\partial_r(rS_{n-1}^m) - nS_{n-1}^m] + (n+2)c_{n+1}^m\,[\partial_r(rS_{n+1}^m) + (n+1)S_{n+1}^m] - imrT_n^m\right|^2.$$

Thus the magnetic energy is not the sum of the toroidal and poloidal energies in $\mathring{V}$ if $e \neq 0$. In $r > 1$,

$$|\mathbf{S}|_{\xi^{-1}}^2 = \xi^2 \sum_{n,m}\{\lambda_n^2|S_n^m|^2 + \lambda_n|\partial_\xi(\xi S_n^m) - 2S_n^m|^2\}$$

$$|\mathring{B}_z|_{\xi^{-1}}^2 = \xi^2 \sum_{n,m} \left|(n-1)c_n^m[\partial_\xi(\xi S_{n-1}^m) + (n-2)S_{n-1}^m] - (n+2)c_{n+1}^m[\partial_\xi(\xi S_{n+1}^m) - (n+3)S_{n+1}^m] - imrT_n^m\right|^2.$$

4 Results

Magnetic free-decay $\mathbf{v} = \mathbf{0}$ provides an excellent test case, since the new features in equations (2.11) and (2.12) are all active if the ellipticity $e > 0$. If $e = 0$, the conducting volume V is spherical with magnetic free-decay modes given by

$$S_n^m = e^{-j_{n-1,k}^2 t} \begin{cases} j_n(j_{n-1,k} r), \\ j_n(j_{n-1,k}) r^{-n-1}, \end{cases} \qquad T_n^m = e^{-j_{n,k}^2 t} \begin{cases} j_n(j_{n,k} r), & r < 1\,; \\ 0, & r > 1\,; \end{cases} \tag{4.1}$$

where $n \geq 1$, j_n is the nth spherical Bessel function of the first kind and $j_{n,k}$ is the kth positive zero of j_n, i.e. $j_n(j_{n,k}) = 0$ for $n = 0, 1, \ldots$, $k = 1, 2, \ldots$. There are n cells of non-zero S or T in latitude and k cells in radius.

4.1 Axisymmetric Free-Decay Solutions

For $e > 0$ there exist analytical axisymmetric ($m = 0$) free-decay ($R = 0$) solutions in terms of spheroidal wave functions using confocal spheroidal coordinates. These functions are difficult to compute even in the arbitrary precision. Further details of the solutions are given in Wu and Roberts (2009). The spheroidal coordinates are also used in §5.

An axisymmetric magnetic field has the representation $\mathbf{B} = \nabla\times(\chi\mathbf{1}_\phi/s) + B_\phi\mathbf{1}_\phi$, where χ is the magnetic flux function, and $\chi = -a^2 cr\sin\theta\,\partial_\theta S$ and $B_\phi = -a\,\partial_\theta T$. The fields χ and B_ϕ are odd (even) in the equator if S and T are even (odd). The associated field $\mathring{\mathbf{B}} = \mathring{\nabla}\times(\mathring{\chi}\mathbf{1}_\phi/\mathring{s}) + \mathring{B}_\phi\mathbf{1}_\phi$, where $\mathring{\chi} = \chi/a^2 c$. Assuming $\chi(\mathbf{r},t) = \hat{\chi}(\mathbf{r})e^{\gamma t}$ and $B_\phi(\mathbf{r},t) = \hat{B}_\phi(\mathbf{r})e^{\gamma t}$, the magnetic induction equation (1.1) with $R_\mathrm{m} = 0$ decouples into two scalar equations of the same form, $\nabla^2 u - 2s^{-1}\partial_s u - \gamma u = 0$, with either $u = \hat{\chi}$ or $u = \hat{B}_\phi$. This equation has separable solutions in confocal oblate spheroidal coordinates (ξ, ϕ, η). The change to (ξ, ϕ, η) from cylindrical polar coordinates (s, ϕ, z) is given by

$$s = d\sqrt{(1+\xi^2)(1-\eta^2)}\,, \quad z = d\xi\eta\,, \quad d := \sqrt{a^2 - c^2} = ae\,. \tag{4.2}$$

The boundary (1.2) is then given by the level surface $\xi = c/d = c/ae$, since $x = s\cos\phi$ and $y = s\sin\phi$. The separable solutions are of the form $u = s\Xi(\xi)H(\eta)$, where $\Xi(\xi) = R_{1n}^{(1)}(-\mathrm{i}\sigma, \mathrm{i}\xi)$ and $H(\eta) = S_{1n}(-\mathrm{i}\sigma, \eta)$ are radial and angular oblate spheroidal wave functions of the first kind, degree n and order 1 (Flammer, 2005, note d differs by a factor 2) and $\sigma^2 = -d^2\gamma$. Since $B_\phi = 0$ on the insulating boundary $\xi = c/ae$, the azimuthal modes are

$$B_\phi = R_{1n}^{(1)}(-\mathrm{i}\sigma_{nk}^\mathrm{a}, \mathrm{i}\xi) S_{1n}(-\mathrm{i}\sigma_{nk}^\mathrm{a}, \eta) e^{\gamma_{nk}^\mathrm{a} t}\,, \tag{4.3}$$

where $\gamma_{nk}^\mathrm{a}(a,c) = -(\sigma_{nk}^\mathrm{a})^2/(a^2 - c^2)$ and σ_{nk}^a is the kth positive zero of $R_{1n}^{(1)}(-i\sigma, ic/ae) = 0$. The field B_ϕ is odd (even) in the equator if n is even (odd) and vanishes in the exterior. The growth rates $\gamma_{nk}^\mathrm{a}(1,c) = \mathring{\gamma}_{nk}^\mathrm{a}(c)$ for $a = 1$ (suppressing $R_\mathrm{m} = 0$), were calculated using the spheroidal wave function package in Mathematica 8 (Falloon et al., 2003). The functions $\mathring{\gamma}_{nk}^\mathrm{a}(c/a)$ for $c/a = 0.01(0.01)0.1(0.05)1$ (see figure 1) are shown in table 3 of Appendix C with $n = 1, 2, 3$, $k = 1$ and $n = 1$, $k = 2$. The relative errors in the numerical eigenvalues are shown in figure 2.

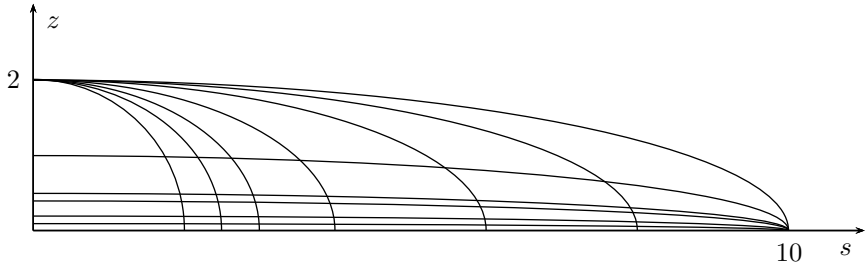

Figure 1: Ellipses of semi-axis ratios $a/c = 1, 1.25, 2, 3, 4, 5$ with $c = 2$ and $a/c = 10, 20, 25, 50, 100$ with $a = 10$.

The meridional solutions are more complicated due to the matching conditions on χ at the conducting boundary $\xi = c/ae$. In the exterior $\xi > c/ae$, $\chi \to 0$ as $\xi \to \infty$, so the separable solutions are $\Xi =$

$R^{(2)}_{1n}(0,\mathrm{i}\xi) = Q^1_n(\mathrm{i}\xi)$ and $H = S_{1n}(0,\eta)P^1_n(\eta)$, where Q^m_n is an associated Legendre function of the second kind,

$$Q^m_n(x) = (x^2-1)^{m/2}\frac{\mathrm{d}^m}{\mathrm{d}x^m}Q_n(x)\,, \quad Q_n(x) = \frac{1}{2}P_n(x)\log\left(\frac{x+1}{x-1}\right) - \sum_{k=1}^{n}\frac{1}{k}P_{k-1}(x)\,P_{n-k}(x)\,,$$

and P_k is the Legendre polynomial (3.2)(b) of degree k. To satisfy the matching conditions, linear combinations of these modes are required,

$$\chi = \begin{cases} \sum_n C_n \dfrac{R^{(1)}_{1n}(-\mathrm{i}\sigma,\mathrm{i}\xi)}{R^{(1)}_{1n}(-\mathrm{i}\sigma,\mathrm{i}c/ae)} S_{1n}(-\mathrm{i}\sigma,\eta)e^{\gamma t}\,, & \xi < c/ae\,; \\ \sum_l \widehat{C}_l \dfrac{Q^1_l(\mathrm{i}\xi)}{Q^1_l(\mathrm{i}c/ae)} P^1_l(\eta)e^{\gamma t}\,, & \xi > c/ae\,. \end{cases} \tag{4.4}$$

Since χ and $\nabla\chi$ are continuous across the conducting boundary,

$$\sum_n C_n d^{1n}_l(-\mathrm{i}\sigma) = \widehat{C}_{l+1}\,, \quad \sum_n C_n \partial_\xi(\log R^{(1)}_{1n}(-\mathrm{i}\sigma,\mathrm{i}\xi)) = \widehat{C}_{l+1}\partial_\xi(\log Q^1_{l+1}(\mathrm{i}\xi))\,, \quad \text{at } \xi = c/ae,$$

using $S_{mn}(-\mathrm{i}\sigma,\eta) = \sum'_{l\geq 0} d^{mn}_l(-\mathrm{i}\sigma)P^m_{l+m}(\eta)$, where the primed summation is over $l = n - m \bmod 2$, and $S_{mn}(0,\eta) = P^m_n(\eta)$. Note $d^{mn}_j(0) = \delta^{n-m}_l$. This yields two homogeneous linear systems $\sum_n A_{ln}(\sigma)C_n = 0$, where $l(\geq 0)$ and $n-1(\geq 0)$ are either both odd or both even, and

$$A_{ln}(\sigma) := \{\xi\partial_\xi(\log R^{(1)}_{1n}(-\mathrm{i}\sigma,\mathrm{i}\xi)) - \xi\partial_\xi(\log Q^1_l(\mathrm{i}\xi))\}d^{1n}_l(-\mathrm{i}\sigma)\,, \quad \xi = c/ae\,.$$

For non-trivial solutions $\det[A_{ln}(\sigma)] = 0$, which determines σ. The χ-modes are even (odd) in the equator if n is odd (even). In the spherical limit $a/c \to 1$, $a \to 1$, $e \to 0$, $\xi = c/ae \to \infty$, $\sigma\xi \to \sqrt{-\gamma}$, $\xi\partial_\xi(\log R^{(1)}_{1n}(-\mathrm{i}\sigma,\mathrm{i}\xi)) \to \sqrt{-\gamma}j'_n(\sqrt{-\gamma})/j_n(\sqrt{-\gamma})$ and $\xi\partial_\xi[\log Q^1_{l+1}(i\xi)] \to -l-2$, using (Flammer, 2005, eq.(4.1.15)) and (Olver et al., 2010, eqs.(14.8.15), (14.3.10)),

$$R^{(1)}_{mn}(-\mathrm{i}\sigma,\mathrm{i}\xi) = N^{-1}_{mn}(1+\xi^{-2})^{1/2}\sum_{l\geq 0}{}' \,\mathrm{i}^{l+m-n}\frac{(l+2m)!}{l!}d^{mn}_l(-\mathrm{i}\sigma)j_{l+m}(\sigma\xi)$$

$$e^{-\mathrm{i}\mu\pi}\frac{Q^\mu_\nu(w)}{\Gamma(\nu+\mu+1)} = \mathbf{Q}^\mu_\nu(w) \sim \frac{\pi^{1/2}}{\Gamma(\nu+\frac{3}{2})(2w)^{\nu+1}}\,, \quad \text{as } |w| \to \infty; \tag{4.5}$$

where the normalisation factor $N_{mn} := \sum'_{l\geq 0} d^{mn}_l(-\mathrm{i}\sigma)(l+2m)!/l!$. Hence as $a/c \to 1$, $A_{ln}(\sigma) \to \sqrt{-\gamma}j_{n-1}(\sqrt{-\gamma})\delta^{n-1}_l/j_n(\sqrt{-$ and $\gamma \to -j^2_{n-1,k}$, $n = 1,2,\ldots$, recovering the $m = 0$ poloidal modes in (4.1). The zeros of $\det[A_{ln}(\sigma)] = 0$ for $e > 0$ and hence the axisymmetric meridional growth rates $\gamma^{\mathrm{m}}_{nk}(a,c)$ can thus be found by continuation from $e = 0$. By continuity the cell structure of the spherical free-decay modes extends to $e > 0$. The growth rates $\gamma^{\mathrm{m}}_{nk}(1,c) = \mathring{\gamma}^{\mathrm{m}}_{nk}(c)$ for $a = 1$ (suppressing $R_{\mathrm{m}} = 0$) were computed in Mathematica 8, but note the angular coefficients d^{1k}_l are not intrinsic functions (Emig et al., 2008, Falloon et al., 2003). The decay rate functions $\mathring{\gamma}^{\mathrm{m}}_{1,1}(c/a)$ and $\mathring{\gamma}^{\mathrm{m}}_{2,1}(c/a)$ are given in table 3 of Appendix C for $c/a = 0.01(0.01)0.1(0.05)1$. The relative errors in the numerical eigenvalues are shown in figure 2. There is excellent agreement with the analytic solutions, but truncation levels must increase substantially for $c/a = 0.01$.

4.2 Free-Decay Solutions for Small Ellipticity

For small ellipticity $e \ll 1$ free-decay solutions can be expanded in powers of e^2. Only the growth rate to first order is calculated here; the modes are derived elsewhere (Ivers, 2017). The degeneracy in the decay rates of S^m_n and T^m_{n-1} splits if $e > 0$ and motivates the following expansion in e^2,

$$T^m_{n-1} = T^m_{n-1,0} + e^2T^m_{n-1,2} + \ldots, \qquad S^m_n = S^m_{n,0} + e^2S^m_{n,2} + \ldots, \qquad \gamma = \gamma_0 + e^2\gamma_2 + \ldots \tag{4.6}$$

$$T^m_{n-1\pm 2l} = T^m_{n-1\pm 2l,2l}e^{2l} + \ldots, \qquad S^m_{n\pm 2l} = S^m_{n\pm 2l,2l}e^{2l} + \ldots, \qquad l \geq 1\,, \tag{4.7}$$

where $\gamma_0 = -\lambda^2$, $T^m_{n-1-2l} = 0$ if $l > (n-1-m)/2$ and $S^m_{n-2l} = 0$ if $l > (n-m)/2$. Let $\lambda = j_{n-1,k}$ and suppress k below. The $l = 0$ terms are spherical free-decay modes: if $r < 1$, $S^m_{n,0} = \sigma j_n(\lambda r)$ and $T^m_{n-1,0} = i\tau j_{n-1}(\lambda r)$, where σ and τ are constants with typically $\sigma\tau \neq 0$; and if $r > 1$, $S^m_{n,0} = \sigma j_n(\lambda)r^{-n-1}$ and $T^m_{n-1,0} = 0$.

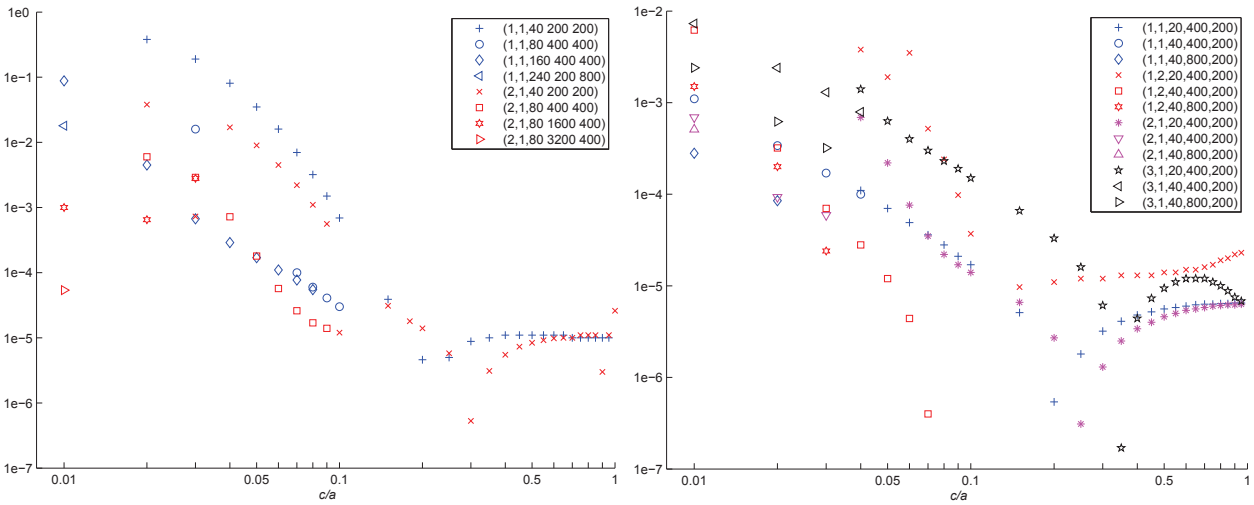

Figure 2: Relative errors of axisymmetric meridional $\gamma^{\rm m}_{nk}$ (left) and azimuthal $\gamma^{\rm a}_{nk}$ (right) free-decay rates versus $0.01 \le c/a \le 1$ at different truncation levels (N, J, J_ξ) for the values of (n, k, N, J, J_ξ) shown.

Substitute expansions (4.6) and (4.7) into the interior equations (3.4) and (3.5), and the exterior equations (3.12) and (3.13). Several useful factors of $1-e^2$, which affect only subdominant terms, are retained for simplicity.

Since $\mathrm{D}_n j_n(\lambda r) = \gamma_0 j_n(\lambda r)$, equations (3.4) and (3.5) are satisfied to $\mathcal{O}(1)$. To $\mathcal{O}(e^2)$ they give, applying the recurrence relations for spherical Bessel functions, $\mathrm{d}_{n+1} j_n(\lambda r) = \lambda j_{n-1}(\lambda r)$ and $\mathrm{d}_{-n} j_n(\lambda r) = -\lambda j_{n+1}(\lambda r)$,

$$(\gamma_0 - \mathrm{D}_{n-1}) T^m_{n-1,2} = -\frac{i}{1-e^2}\left\{\frac{2mc^m_n}{n(n-1)}\sigma\gamma_0\lambda - (C^m_{n-1}\gamma_0 - \widetilde{\gamma}_2)\tau\right\} j_{n-1}(\lambda r) \tag{4.8}$$

$$(\gamma_0 - \mathrm{D}_n) S^m_{n,2} = \frac{1}{1-e^2}\left\{(C^m_n\gamma_0 - \widetilde{\gamma}_2)\sigma + \frac{2mc^m_n}{n(n+1)}\tau\lambda\right\} j_n(\lambda r)\,, \tag{4.9}$$

where $\widetilde{\gamma}_2 := \gamma_2(1-e^2)$ and C^m_n is given by (3.9). In the exterior $r > 1$, the $\mathcal{O}(e^2)$ equations from (3.12) and (3.13) yield

$$T^m_{n-1,2} = \frac{im(n+1)c^m_n}{(n-1)n}\mathrm{d}_{n+1} S^m_{n,0} = 0\,, \quad \mathrm{D}_n S^m_{n,2} = \widehat{C}^m_n \mathrm{D}_n S^m_{n,0} = 0\,. \tag{4.10}$$

Hence the boundary and matching conditions (3.3) imply the boundary conditions,

$$T^m_{n-1,2} = 0\,, \quad \mathrm{d}_{n+1} S^m_{n,2} = 0\,, \quad \text{at } r = 1-. \tag{4.11}$$

To find the growth rate multiply (4.8) by $r^2 j_{n-1}(\lambda r)$, (4.9) by $r^2 j_n(\lambda r)$, and integrate r over $[0,1]$. Two integrations by parts, the boundary conditions (4.11), $(\gamma_0 - \mathrm{D}_p) j_p(\lambda r) = 0$ and $\int_0^1 r^2 j_p^2(\lambda r)\,\mathrm{d}r \ne 0$ yield the solvability conditions

$$\frac{2mc^m_n}{n(n-1)}\sigma\gamma_0\lambda - (C^m_{n-1}\gamma_0 - \widetilde{\gamma}_2)\tau = 0\,, \quad (C^m_n\gamma_0 - \widetilde{\gamma}_2)\sigma + \frac{2mc^m_n}{n(n+1)}\tau\lambda = 0\,.$$

If $\sigma\tau \ne 0$, $(C^m_{n-1} - \widetilde{\gamma}_2/\gamma_0)(C^m_n - \widetilde{\gamma}_2/\gamma_0) = (2mc^m_n)^2/[(n^2-1)n^2]$. Thus $\gamma = {}^{\pm}\gamma^m_n(e) + O(e^4)$ where

$${}^{\pm}\gamma^m_n(e) := \gamma_0 + \frac{e^2\widetilde{\gamma}_2}{1-e^2}\,, \quad \frac{\widetilde{\gamma}_2}{\gamma_0} = \tfrac{1}{2}(C^m_{n-1}+C^m_n) \pm \tfrac{1}{2}\sqrt{(C^m_n - C^m_{n-1})^2 + \frac{(4mc^m_n)^2}{(n^2-1)n^2}} > 0\,. \tag{4.12}$$

If $e > 0$, ${}^{+}\gamma^m_n(e) > {}^{-}\gamma^m_n(e)$. Since ${}^{\pm}\gamma^{-m}_n = {}^{\pm}\gamma^m_n$ we consider only $m \ge 0$. If $m = n$ there is one non-trivial root, $\widetilde{\gamma}_2/\gamma_0 = C^n_n = (n+3)/[(n+1)(2n+3)]$ and $\tau = 0$. If $m = 0$, either $\sigma = 0$ and $\widetilde{\gamma}_2/\gamma_0 = C^0_{n-1}$, or $\tau = 0$ and $\widetilde{\gamma}_2/\gamma_0 = C^0_n$. Thus, for $n > 1$ and $k \ge 1$ (restoring k) there $2n+1$ modes: ${}^{-}\gamma^m_{nk}$ for $m = 0 : n-1$ and ${}^{+}\gamma^m_{nk}$ for $m = 0 : n$; for $n = 1$ there are two modes, ${}^{-}\gamma^0_{1,k}$ and ${}^{+}\gamma^1_{1,k}$. Figure 3 compares computed values of γ with ${}^{\pm}\gamma^m_{4,1}$ and the zero $j_{3,1} \approx 6.98793$ on $0 \le e \le 0.4$, i.e. $\gamma_0 = -48.8312$ and $1 \le a/c \le 5/\sqrt{21} \approx 1.09$. Using an averaged sub-dominant denominator $1 - \frac{1}{2}e^2$ gives better agreement than either $1-e^2$ or 1 for e near 0.4.

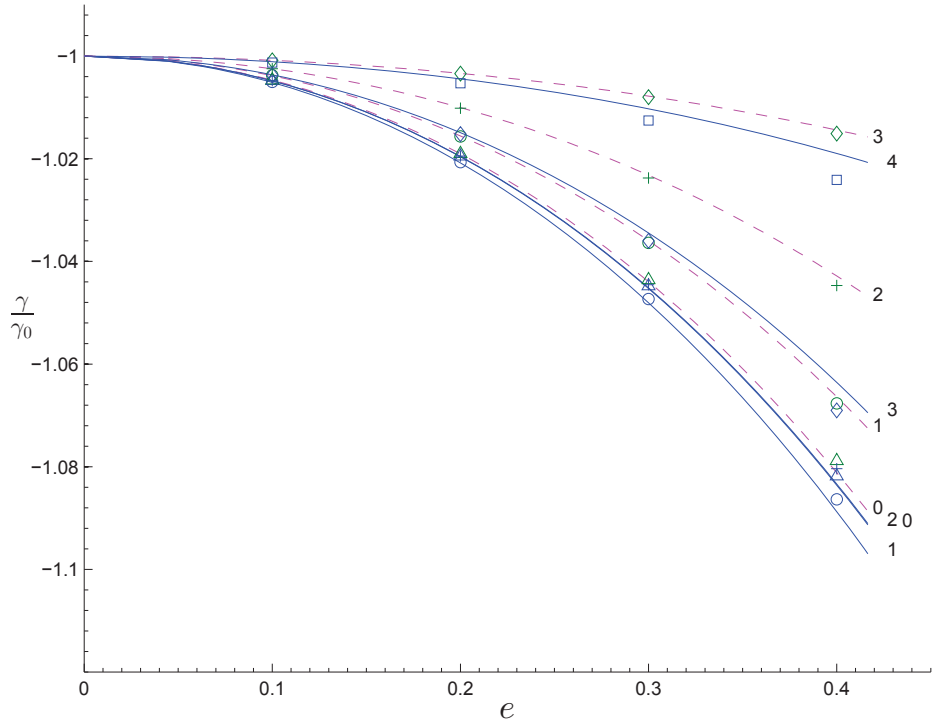

Figure 3: Splitting of free-decay modes. Comparison of computed γ with (4.12) for small ellipticity $0 \le e \le 0.4$. Solid and broken curves are ${}^{\pm}\gamma^{m}_{4,1}$ with averaged denominator. Symbols $\triangle$, $\circ$, $+$, $\diamond$, $\square$ are computed values with $(N, J, J_\xi) = (20, 800, 200)$ for $m = 0, 1, 2, 3, 4$. The ${}^{+}\gamma^{0}_{4,1}$ and ${}^{+}\gamma^{2}_{4,1}$ curves are different.

4.3 Non-Axisymmetric Free-Decay Solutions

The $n = 1$, $k = 1$ modes are ${}^{-}\gamma^{0}_{1,1} = -(\frac{4}{5} + \frac{1}{5}(a/c)^2)\pi^2 + \mathcal{O}(e^4) = \mathring{\gamma}^{\rm m}_{1,1}$, shown in table 3 for $0.01 \le c/a \le 1$ and ${}^{+}\gamma^{1}_{1,1} = -(\frac{3}{5} + \frac{2}{5}(a/c)^2)\pi^2 + \mathcal{O}(e^4)$, shown in table 2 for $1 \le a/c \le 25$. For $a/c = 1.01$, the leading term gives ${}^{+}\gamma^{1}_{1,1} \approx -9.94896$ compared to the eigenvalue -9.94890 computed with $(N, J, J_\xi) = (40, 400, 200)$; for $a/c = 1.1$, ${}^{+}\gamma^{1}_{1,1} \approx -10.699$ compared to the eigenvalue -10.695. Typical spherical harmonic coefficients are shown in figure 4. Since $\mathbf{B} = \mathbf{0}$ if and only if $\mathring{\mathbf{B}} = \mathbf{0}$ at a point, a magnetically hidden dynamo occurs only if $\mathring{\mathbf{B}} = \mathbf{0}$ in $E^3 \setminus V$. Unlike the sphere the only hidden free-decay modes in a spheroid are the $m = 0$ toroidal modes.

4.4 Dynamos with Axisymmetric Flows

The dynamo action of three axisymmetric flows is now considered for aspect ratios $1 \le a/c \le 25$. These three flows are constructed by choosing as $\mathring{\mathbf{v}}$ in $\mathring{V}$ three spherical flows of Dudley and James (1989) which exhibit dynamo action, and transforming them to kinematically feasible spheroidal flows $\mathbf{v}$ in V [see the discussion following (2.14)]. Axisymmetry of $\mathring{\mathbf{v}}$ is preserved under the transformation to $\mathbf{v}$ if the symmetry axes of $\mathring{\mathbf{v}}$ and the spheroid V are aligned. In cylindrical polar coordinates (s, ϕ, z) and $(\mathring{s}, \phi, \mathring{z})$ with common unit vectors $(\mathbf{1}_s, \mathbf{1}_\phi, \mathbf{1}_z)$, where s is the physical cylindrical radius, the scale transformation (2.4) is $s = a\mathring{s}$, $z = c\mathring{z}$, $v_s = a\mathring{v}_s$, $v_\phi = a\mathring{v}_\phi$ and $v_z = c\mathring{v}_z$. An incompressible axisymmetric flow has the meridional-azimuthal representation $\mathbf{v} = \mathbf{v}_{\rm m} + \omega s \mathbf{1}_\phi$ where $\mathbf{v}_{\rm m} = \nabla \times (\psi \mathbf{1}_\phi / s)$, and $\mathring{\mathbf{v}} = \mathring{\mathbf{v}}_{\rm m} + \mathring{\omega}(\mathring{s}, \mathring{z})\mathring{s}\mathbf{1}_\phi$ where $\mathring{\mathbf{v}}_{\rm m} = \mathring{\nabla} \times (\mathring{\psi}\mathbf{1}_\phi/\mathring{s})$. Hence the stream functions and differential rotations are related by $\psi(s, z) = a^2 c \mathring{\psi}(s/a, z/c)$ and $\omega(s, z) = \mathring{\omega}(s/a, z/c)$. The Dudley and James (1989) spherical dynamo flows are of the form

$$\mathring{\mathbf{v}} = \epsilon \mathring{\nabla} \times \left(\frac{\mathring{\psi}}{r \sin\theta} \mathbf{1}_\phi \right) + \mathring{\omega} r \sin\theta \, \mathbf{1}_\phi \,,$$

where ϵ is a tuning parameter (Latter and Ivers, 2010). The associated toroidal-poloidal velocity potentials t and s are given by $\partial_\theta s = -\mathring{\psi}/r \sin\theta$ and $\partial_\theta t = -\mathring{\omega} r \sin\theta$. If $\mathring{\psi}_1 := r \sin \pi r \sin^2\theta$, $\mathring{\psi}_2 := 3r^2 \sin \pi r \sin^2\theta \cos\theta$,

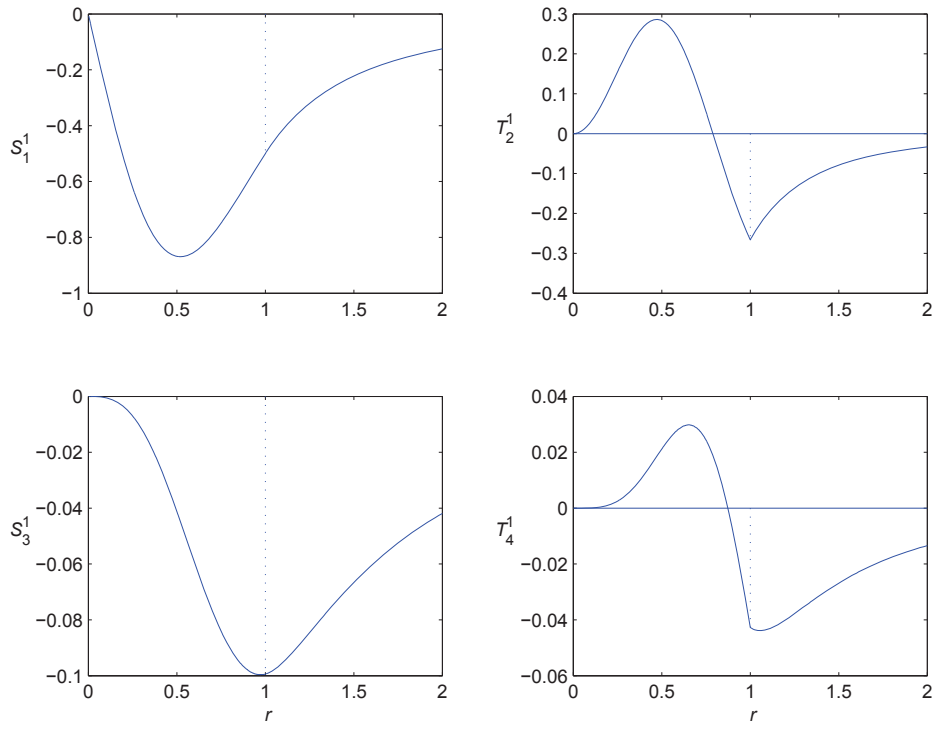

Figure 4: The $S_1^1(r)$ and $T_n^1(r)$ coefficient functions of ${}^+\gamma_{1,1}^1$ for $n \le 4$. The toroidal coefficients T_2^1, T_4^1 are non-zero in the insulating exterior $r > 1$ and their first derivatives have a jump discontinuity at $r = 1$.

$\mathring{\omega}_1 := r^{-1}\sin\pi r$, $\mathring{\omega}_2 := 3\sin\pi r\,\cos\theta$, the three flows are $(\mathring{\psi}_1, \mathring{\omega}_1)$, $(\mathring{\psi}_2, \mathring{\omega}_1)$, $(\mathring{\psi}_2, \mathring{\omega}_2)$ with $\epsilon = 0.17, 0.13, 0.14$ respectively, i.e. in toroidal-poloidal form,

(a) s_1t_1-flow: $s = t = \sin\pi r\,\cos\theta$, $s_1^0 = t_1^0 = \frac{1}{\sqrt{3}}\sin\pi r$, $\epsilon = 0.17$;

(b) s_2t_1-flow: $s = \frac{3}{2}r\sin\pi r\cos^2\theta$, $t = \sin\pi r\,\cos\theta$, $s_2^0 = \frac{1}{\sqrt{5}}r\sin\pi r$, $t_1^0 = \frac{1}{\sqrt{3}}\sin\pi r$, $\epsilon = 0.13$;

(c) s_2t_2-flow: $s = t = \frac{3}{2}r\sin\pi r\cos^2\theta$, $s_2^0 = t_2^0 = \frac{1}{\sqrt{5}}r\sin\pi r$, $\epsilon = 0.14$;

using $Y_1^0 = \sqrt{3}\cos\theta$ and $Y_2^0 = \sqrt{5}(-1 + 3\cos^2\theta)/2$. The flows are shown in figure 5 for $a/c = 5$.

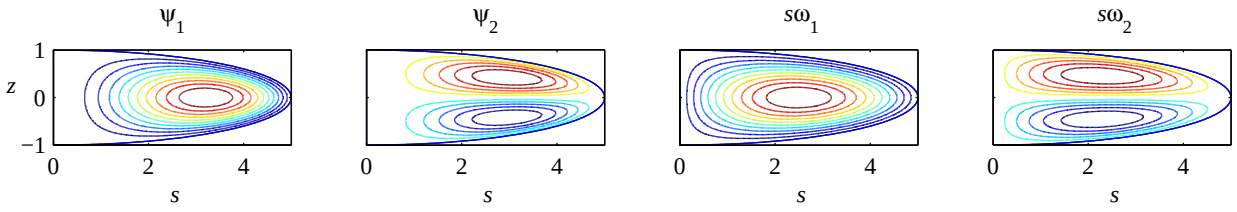

Figure 5: Stream functions ψ_1, ψ_2 and azimuthal velocities $s\mathring{\omega}_1$ and $s\mathring{\omega}_2$ for $a/c = 5$.

Since the velocities are axisymmetric the magnetic field decouples into toroidal-poloidal chains $S_m^m, T_m^m, S_{m+1}^m, T_{m+1}^m, \ldots$ for $m = 0, 1, 2, \ldots$ (omit S_0^0, T_0^0). The s_2t_1-flow is equatorially symmetric (ES), i.e. it has a chain of the form $t_1^0, s_2^0, t_3^0, s_4^0, \ldots$, so the magnetic field decouples into an equatorially anti-symmetric (EA) field with the chain $T_m^m, S_{m+1}^m, T_{m+2}^m, \ldots$ or an ES field with the chain $S_m^m, T_{m+1}^m, S_{m+2}^m, \ldots$. The s_1t_1- and s_2t_2-flows are not ES so the magnetic field has no EA/ES symmetry. Numerically the coefficient chains are truncated at degree N. Critical dynamo solutions with $\mathrm{Re}\,\gamma = 0 = \mathrm{Re}\,\mathring{\gamma}$ are computed. Results for the three flows are shown in figure 6 and in table 2. For a sphere ($a/c = 1$) the critical magnetic Reynolds number and

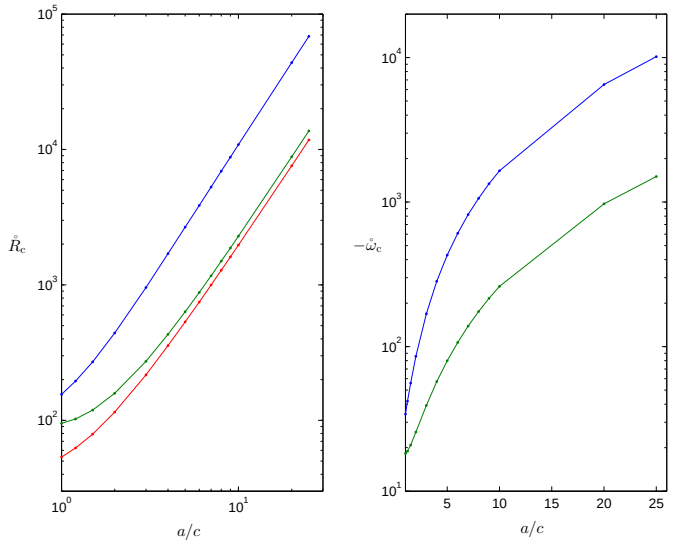

Figure 6: Critical magnetic Reynolds numbers $\mathring{R}_c$ and angular frequency $\mathring{\omega}_c$ vs $a/c = 5$ for the flows (top to bottom) s_1t_1, s_2t_1 and s_2t_2 ($\mathring{R}_c$ only).

frequency are consistent with Dudley and James (1989). The slopes of the magnetic Reynolds number plots for $a/c \geq 5$ indicate $\mathring{R}_c \propto (a/c)^{2.0}$ for s_1t_1, and $\mathring{R}_c \propto (a/c)^{1.9}$ for s_2t_1 and s_2t_2. Truncation levels (N, J, J_ξ) were: for the s_1t_1 flow, $(80, 800, 100)$ for $a/c = 3, 4$, $(80, 800, 200)$ for $5 \leq a/c < 10$ and $(80, 1600, 200)$ for $10 \leq a/c \leq 25$; for the s_2t_1 flow, $(80, 800, 100)$ for $a/c < 5$ and $(80, 800, 200)$ for $a/c \geq 5$; and for the s_2t_2 flow, $(80, 800, 200)$.

v	**0**	s_1t_1		s_2t_1		s_2t_2
a/c	${}^{+}\gamma^1_{1,1}$	$\mathring{R}_c$	$\mathrm{Im}\,\mathring{\gamma}_c$	$\mathring{R}_c$	$\mathrm{Im}\,\mathring{\gamma}_c$	$\mathring{R}_c$
1	$-\pi^2$	155.585	−34.1440	94.9263	−18.2102	53.5624
1.2	−11.592	194.942	−41.9226	102.3607	−18.9060	62.4924
1.5	−14.689	270.313	−55.986	119.2005	−20.8543	79.1692
2	−21.108	441.614	−85.738	158.6265	−25.6386	115.1571
3	−38.223	957.444	−168.675	273.0472	−39.1726	216.5595
4	−60.643	1701.689	−283.199	431.8008	−57.2683	356.0900
5	−88.189	2671.595	−429.725	633.9955	−79.8498	533.0085
6	−120.80	3865.436	−608.442	879.4256	−106.970	746.9163
7	−158.45	5282.018	−819.416	1167.983	−138.665	997.5940
8	−201.11	6920.498	−1062.669	1499.612	−174.961	1284.916
9	−248.79	8780.251	−1338.204	1874.280	−215.874	1608.804
10	−301.46	10860.64	−1646.07	2291.963	−261.412	1969.214
20	−1102	43782.25	−6501.62	8832.98	−972.20	7578.5
25	−1689	68486.7	−10141.2	13715.5	−1502.2	11750

Table 2: Critical magnetic Reynold's number $\mathring{R}_c$ vs a/c for the s_1t_1 and s_2t_2 flows with $m = 1$ magnetic fields, and the s_2t_1 flow with an EA (no ES dynamo has been found) $m = 1$ magnetic field. For most aspect ratios $(N, J, J_\xi) = (20, 200, 50)$. For the s_2t_2 flow $\mathrm{Im}\,\mathring{\gamma}_c = 0$.

Magnetic field plots are constructed for the normal, tangential and azimuthal components in the natural orthonormal basis $(\mathbf{1}_n, \mathbf{1}_t, \mathbf{1}_\phi)$, $\mathbf{B} = B_n\mathbf{1}_n + B_t\mathbf{1}_t + B_a\mathbf{1}_\phi$. Geometrically, $\mathbf{1}_n$ and $\mathbf{1}_t$ are normal and tangent to the r-surface at any point, and lie in the meridional plane. This is a hybrid non-coordinate basis since $\mathbf{1}_n = \mathbf{e}^1/|\mathbf{e}^1| = \mathbf{n}/|\mathbf{n}|$, $\mathbf{1}_t = \mathbf{e}_2/|\mathbf{e}_2| = \mathbf{e}_\theta/|\mathbf{e}_\theta|$ and $\mathbf{1}_\phi = \mathbf{e}^3/|\mathbf{e}^3| = \mathbf{e}_3/|\mathbf{e}_3| = \mathbf{e}_\phi/|\mathbf{e}_\phi|$. Now $|\mathbf{n}|B_n = \mathbf{n}\cdot\mathbf{B} = \mathring{\mathbf{r}}\cdot\mathbf{L}\cdot\mathbf{B} = \mathring{\mathbf{r}}\cdot\mathring{B} = r\mathring{B}_r$, thus $B_n = r\mathring{B}_r/|\mathbf{n}|$, where $ac|\mathbf{n}| = r\sqrt{a^2\cos^2\theta + c^2\sin^2\theta}$. Also, since $\mathbf{B} = \mathring{B}_r\mathbf{e}_r + \mathring{B}_\theta\mathbf{e}_\theta + \mathring{B}_\phi\mathbf{e}_\phi$, $B_t = \mathbf{1}_t\cdot\mathbf{B} = \mathring{B}_r\mathbf{1}_t\cdot\mathbf{e}_r + \mathring{B}_\theta\mathbf{1}_t\cdot\mathbf{e}_\theta$, where $\mathbf{1}_t\cdot\mathbf{e}_r = \mathbf{e}_1\cdot\mathbf{e}_\theta/|\mathbf{e}_\theta| = (a^2-c^2)\sin\theta\,\cos\theta/|\mathbf{e}_\theta|$

and $\mathbf{1}_\mathrm{t}\cdot\mathbf{e}_\theta = |\mathbf{e}_\theta| = \sqrt{a^2\cos^2\theta + c^2\sin^2\theta}$. Lastly, $B_\mathrm{a} = c\mathring{B}_\phi$. The components $\mathring{B}_r$, $\mathring{B}_\theta$, $\mathring{B}_\phi$ are computed from T and S in $\mathring{E}^3$ as in the spherical case. The critical magnetic fields of the s_1t_1-flow are shown in figure 7 for $a/c = 10$ and figure 8 for $a/c = 5$. Strong magnetic field is confined near the axis with very weak field towards the periphery of the spheroid, both internally and externally. The fields are reminiscent of the spherical results of Latter and Ivers (2010) at much larger magnetic Reynolds numbers. The critical fields of the s_2t_1-flow and s_2t_2-flow for $a/c = 5$ are shown in figures 9 and 10 respectively. Strong magnetic field occurs toward the periphery for the s_2t_1-flow, both internally and externally. For the s_2t_2-flow, internally the strongest magnetic field occurs near the axis but there is also strong field toward the periphery; externally the strongest field occurs at the periphery.

5 Alternative Methods for the Insulating Exterior

Two alternative solution methods for the insulating exterior are given in this section. The first method eliminates T_n^m from the system of exterior equations. Solving (3.12) for T_n^m gives

$$T_n^m = \frac{\mathrm{i}me^2}{\lambda_n - e^2m^2}\{-(n-1)c_n^m\mathrm{d}_{1-n}S_{n-1}^m + (n+2)c_{n+1}^m\mathrm{d}_{n+2}S_{n+1}^m\}\,, \quad \text{in } r \geq 1-. \tag{5.1}$$

Observe from the matching conditions (3.3) on T_n^m and S_n^m that equation (5.1) holds at $r = 1\pm$. Also, since $|m| \leq n$ and $e^2 < 1 < n(n+1)/m^2$, $\lambda_n \neq e^2m^2$, there are no zero divisors. There is a simpler equation than (3.12) for $m \neq 0$, the spectral form of (2.20),

$$-(n-1)c_n^m\mathrm{d}_{1-n}T_{n-1}^m + (n+2)c_{n+1}^m\mathrm{d}_{n+2}T_{n+1}^m + im\mathrm{D}_nS_n^m = 0\,, \tag{5.2}$$

which can be derived from (2.29) and used with (5.1). However, explicit elimination of $T_{n\pm1}^m$ from (5.2) or (3.13) using (5.1) gives

$$\mathrm{D}_nS_n^m + e^2\bigg\{\frac{(n-2)(n-1)}{\lambda_{n-1}-e^2m^2}c_{n-1,n}^m\mathrm{D}_{1-n,2-n}S_{n-2}^m - \frac{(n-1)(n+1)}{\lambda_{n-1}-e^2m^2}c_{n,n}^m\mathrm{D}_nS_n^m$$
$$-\frac{n(n+2)}{\lambda_{n+1}-e^2m^2}c_{n+1,n+1}^m\mathrm{D}_nS_n^m + \frac{(n+2)(n+3)}{\lambda_{n+1}-e^2m^2}c_{n+1,n+2}^m\mathrm{D}_{n+2,n+3}S_{n+2}^m\bigg\} = 0\,. \tag{5.3}$$

Equation (5.3), which is valid for all m, can be used in $r > 1$ together with (5.1) at $r = 1-$.

The second method replaces the system of equations for T_n^m and S_n^m in the exterior by a coupled system of boundary conditions at $r = 1-$, derived from (5.1) and relations between the scalar, toroidal and poloidal potentials Ψ, T and S. Laplace's equation $\nabla^2\Psi = 0$ separates in the confocal oblate spheroidal coordinates (4.2). The exterior solution is

$$\Psi = \sum_{n\geq1,m}\Psi_n^mQ_n^m(\mathrm{i}\xi)P_n^m(\eta)e^{\mathrm{i}m\phi}\,, \quad \text{in } \xi > c/d. \tag{5.4}$$

The homoeoidal coordinates (2.1) and confocal coordinates (4.2) are related by $s = ar\sin\theta = d\sqrt{1+\xi^2}\sqrt{1-\eta^2}$ and $z = c\cos\theta = d\xi\eta$. Solving for r and θ gives

$$r^2 = \frac{d^2}{a^2}(1+\xi^2)(1-\eta^2) + \frac{d^2}{c^2}\xi^2\eta^2\,, \quad \tan\theta = \frac{c}{a}\frac{\sqrt{1+\xi^2}\sqrt{1-\eta^2}}{\xi\eta}\,.$$

The r- and ξ-surfaces coincide if and only if the first equation holds for all $|\eta| \leq 1$. This is true if and only if $r^2/d^2 = (1+\xi^2)/a^2 = \xi^2/c^2$, i.e. $\xi = c/ae$ and $r = \xi d/c = 1$. Thus only the boundary spheroid Σ is both an r-surface and an ξ-surface.

The vector field $\mathbf{n}$ defined in (1.2) is normal to r-surfaces and can be written in the form $\mathbf{n} = \mathbf{1}_sr\sin\theta/a + \mathbf{1}_zr\cos\theta/c$. On Σ, $r = 1$ and $\mathbf{n} = \mathbf{1}_s\sin\theta/a + \mathbf{1}_z\cos\theta/c$. The confocal ξ basis vector $\mathbf{e}_\xi := \partial_\xi\mathbf{r} = d(\xi\sqrt{1-\eta^2}\mathbf{1}_s + \eta\sqrt{1+\xi^2}\mathbf{1}_z)/\sqrt{1+\xi^2}$ is normal to the ξ-surface at any point. In fact, $\mathbf{e}_\xi = cd\mathbf{n}$ on Σ where $\xi = c/ae$ and $\eta = \cos\theta$. Thus, using (2.6), $\partial_\xi\Psi = \mathbf{e}_\xi\cdot\nabla\Psi = -\mathbf{e}_\xi\cdot\mathbf{B} = -cd\mathbf{n}\cdot\mathbf{B} = -cd\mathring{\mathbf{r}}\cdot\mathring{\mathbf{B}} = cd\mathring{\Lambda}^2S$. Thus from (5.4),

$$\Psi_n^mQ_n^{m\prime}(\mathrm{i}c/ae) = \mathrm{i}ace\lambda_nS_n^m\,, \tag{5.5}$$

where the prime indicates the derivative. A second relation between Ψ, S and T is given by the horizontal divergence of $\mathring{\nabla}\Psi = -\mathbf{D}^{-1}\cdot\mathring{\mathbf{B}}$. Using (2.16)(b) and $\mathring{\Lambda}^2 \equiv (r\mathring{\nabla}_\mathrm{h})^2$,

$$\mathring{\Lambda}^2\Psi = -a^2r^2\mathring{\nabla}_\mathrm{h}\cdot(\mathring{\mathbf{B}} - e^2\mathring{B}_z\mathbf{1}_z)_\mathrm{h} = -a^2\mathring{\Lambda}^2\partial_r(rS) + e^2a^2r^2\mathring{\nabla}_\mathrm{h}\cdot(\mathring{B}_z\mathbf{1}_z)_\mathrm{h}\,. \tag{5.6}$$

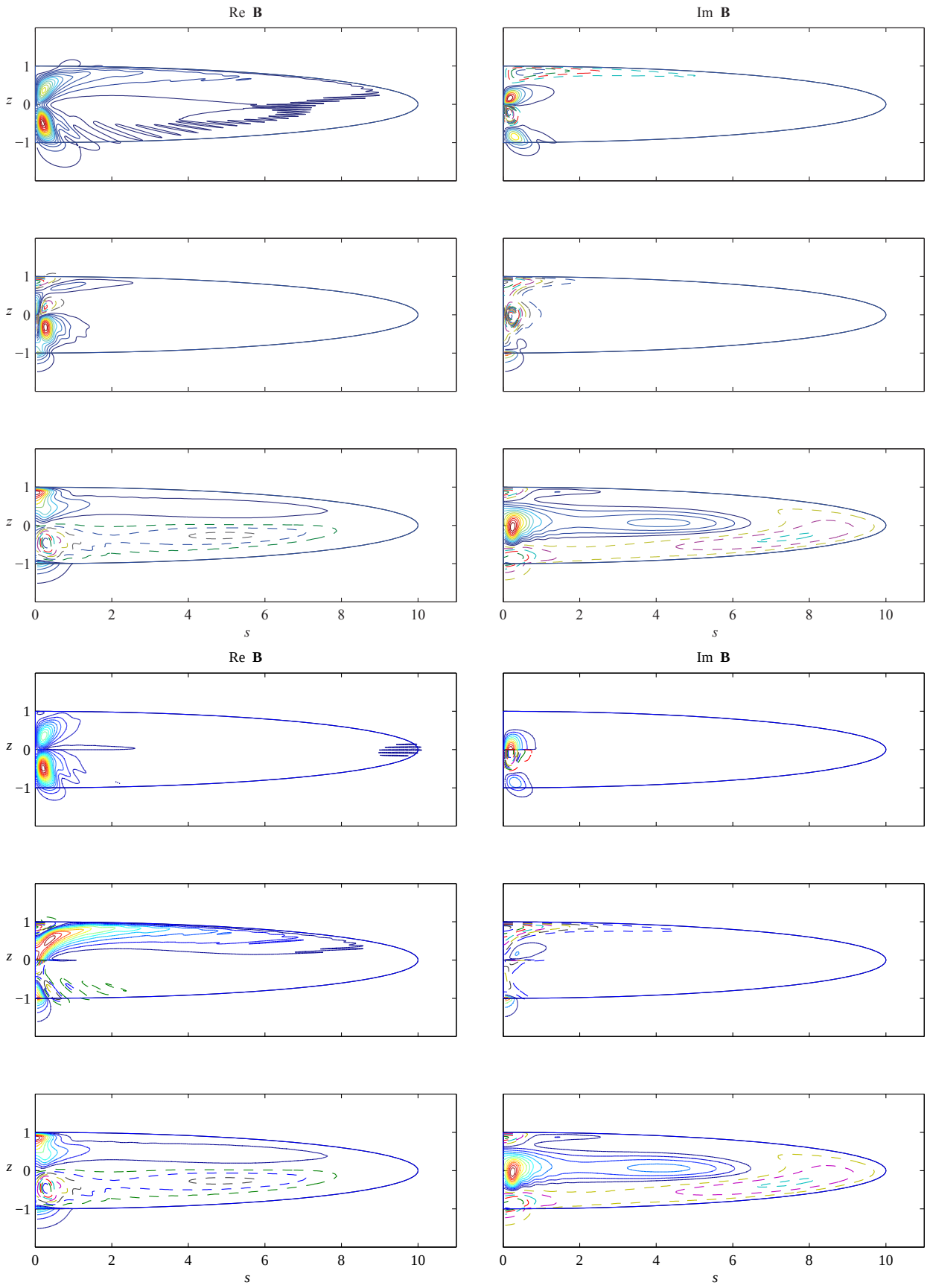

Figure 7: Critical magnetic field for the s_1t_1 flow with $a/c = 10$. Real (left) and imaginary (right) parts of B_r, B_θ, B_ϕ in E^3 (top three rows) and of B_n, B_t, B_a (bottom three rows).

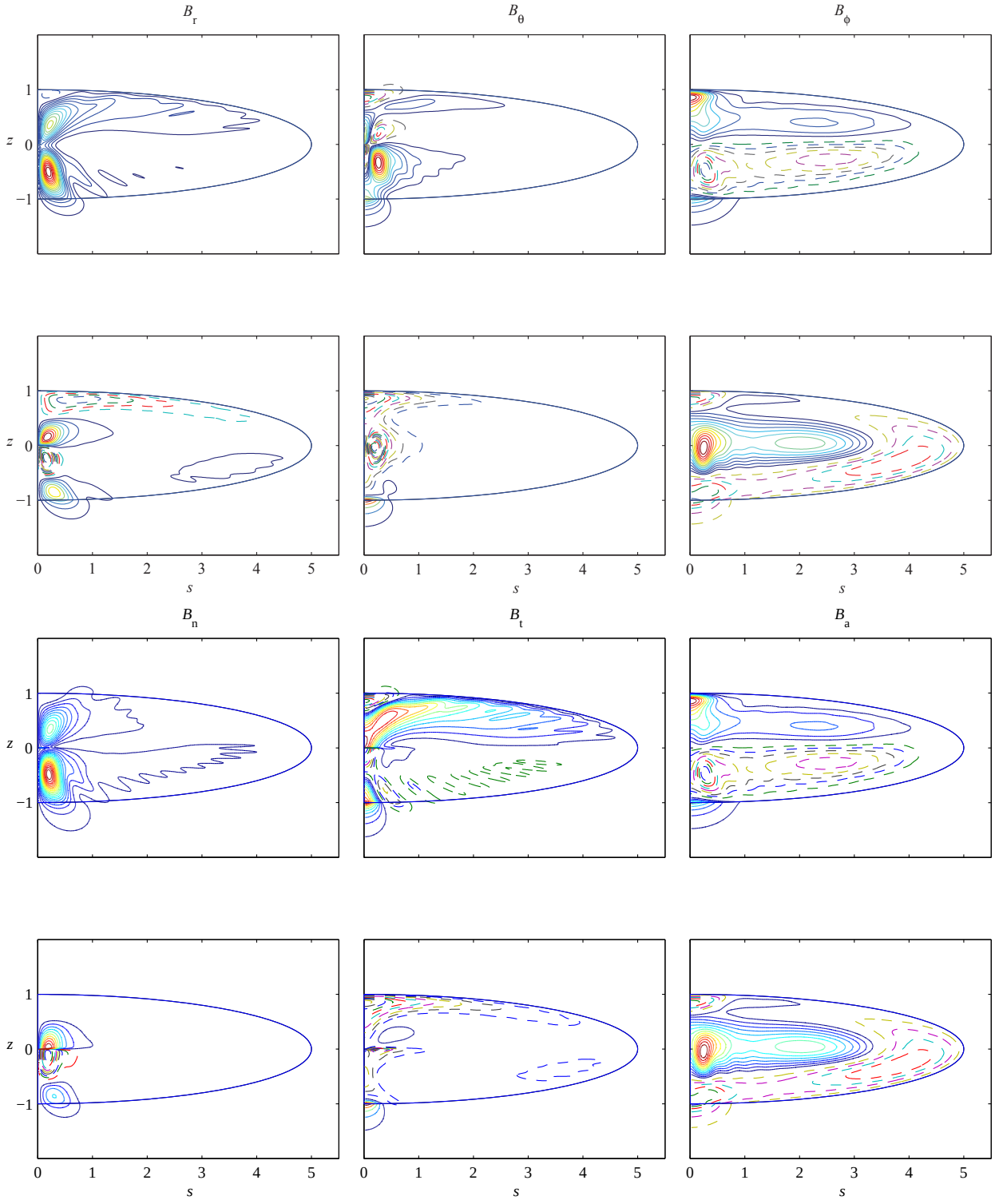

Figure 8: Critical magnetic field for the s_1t_1 flow with $a/c = 5$. Real and imaginary parts of B_r, B_θ, B_ϕ in E^3 (top two rows) and of B_n, B_t, B_a (bottom two rows).

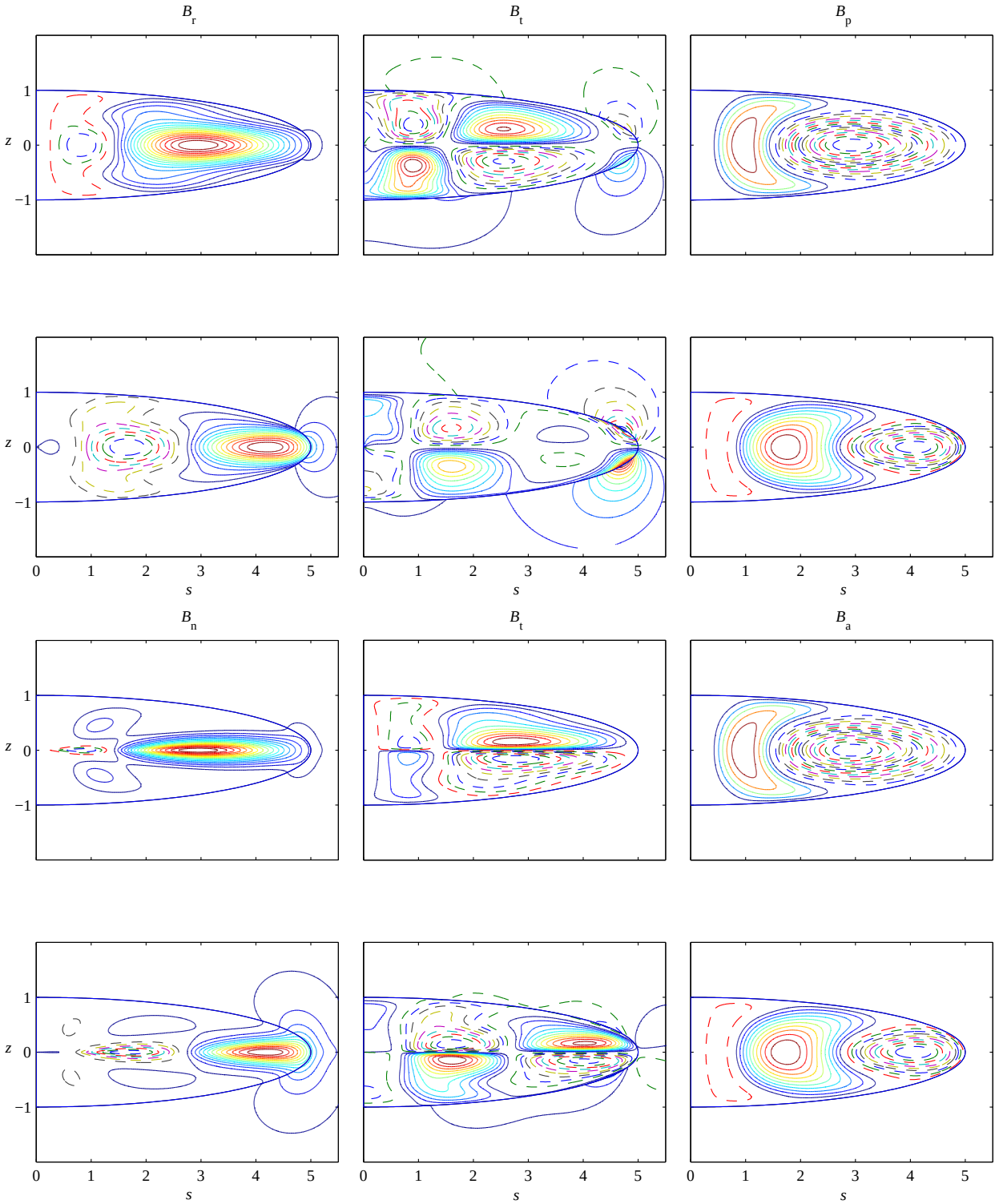

Figure 9: As in figure 8 but for the s_2t_1 flow.

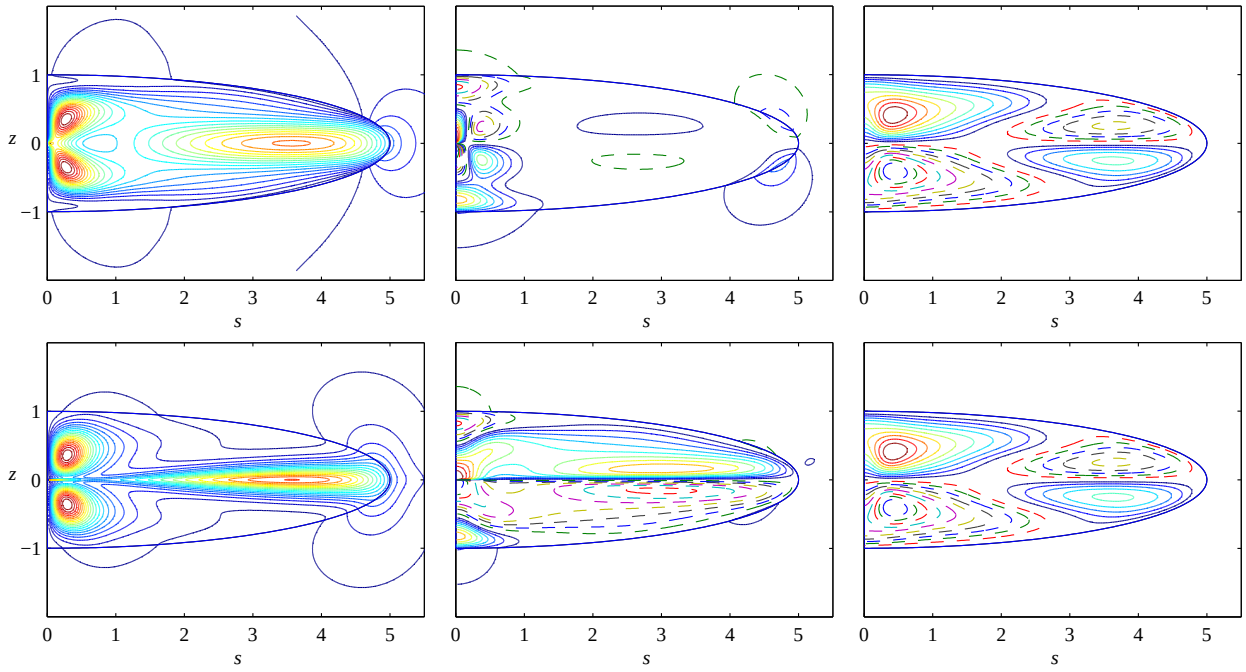

Figure 10: Critical magnetic field for the s_2t_2 flow with $a/c = 5$. Fields B_r, B_θ, B_ϕ in E^3 (top) and B_n, B_t, B_a (bottom).

Substituting (5.4) and evaluating (5.6) on Σ ($\xi = c/ae$, $\eta = \cos\theta$ and $r = 1$) gives

$$\partial_r S_n^m + S_n^m + a^{-2}\Psi_n^m Q_n^m(\mathrm{i}c/ae) = e^2 \mathcal{H}_n^m\{\mathring{B}_z \mathbf{1}_z\}\,, \tag{5.7}$$

introducing the horizontal divergence transform defined by

$$\mathcal{H}_n^m\{\mathbf{F}\} := -\frac{1}{4\pi\lambda_n}\oint Y_n^{m*} r\mathring{\nabla}_{\mathrm{h}}\cdot\mathbf{F}_{\mathrm{h}}\,\mathrm{d}\mathring{\Omega}\,. \tag{5.8}$$

Eliminating Ψ_n^m from (5.5) and (5.8) yields the boundary condition

$$\partial_r S_n^m + \left(1 + e^2\lambda_n \frac{(\mathrm{i}c/ae)Q_n^m(\mathrm{i}c/ae)}{Q_n^{m\prime}(\mathrm{i}c/ae)}\right) S_n^m = e^2\mathcal{H}_n^m\{\mathring{B}_z\mathbf{1}_z\}\,. \tag{5.9}$$

As $a/c \to 1$, $e \to 0$ and the condition (5.9) reduces to the spherical poloidal insulating boundary condition $\partial_r S_n^m + (n+1)S_n^m/r = 0$, since (Olver et al., 2010, equations(14.3.10),(14.8.15))

$$e^{-\mathrm{i}\mu\pi}\frac{Q_\nu^\mu(w)}{\Gamma(\nu+\mu+1)} = \mathbf{Q}_\nu^\mu(w) \sim \frac{\pi^{1/2}}{\Gamma(\nu+\frac{3}{2})(2w)^{\nu+1}}\,, \quad \text{as } |w| \to \infty..$$

The horizontal divergence of $f\mathbf{1}_z$ for a scalar field f is given by $r\nabla_{\mathrm{h}}\cdot(f\mathbf{1}_z)_{\mathrm{h}} = -\sin\theta\,\partial_\theta f - 2\cos\theta\, f$. Thus by (3.10) the spherical harmonic expansion for the horizontal divergence of $f\mathbf{1}_z$ is given by $r\nabla_{\mathrm{h}}\cdot(f\mathbf{1}_z)_{\mathrm{h}} = -\sum_{n,m}\{(n+1)c_n^m f_{n-1}^m - nc_{n+1}^m f_{n+1}^m\}Y_n^m$. Setting $f = \mathring{B}_z$ and using (3.11) yields

$$\begin{aligned}\mathcal{H}_n^m\{\mathring{B}_z\mathbf{1}_z\} = \frac{1}{\lambda_n}\{(n+1)c_n^m[-(n-2)c_{n-1}^m d_{2-n}S_{n-2}^m - imT_{n-1}^m + (n+1)c_n^m d_{n+1}S_n^m] \\ - nc_{n+1}^m[-nc_{n+1}^m d_{-n}S_n^m - imT_{n+1}^m + (n+3)c_{n+2}^m d_{n+3}S_{n+2}^m]\}\,.\end{aligned} \tag{5.10}$$

There is a third relation between Ψ, S and T given by the surface curl of $\mathring{\nabla}\Psi = -\mathbf{D}^{-1}\cdot\mathring{\mathbf{B}}$: if $\mathring{\boldsymbol{\Lambda}} := \mathring{\mathbf{r}}\times\mathring{\nabla}$, then $0 = \boldsymbol{\Lambda}\cdot\mathring{\nabla}\Psi = -\boldsymbol{\Lambda}\cdot(\mathbf{D}^{-1}\cdot\mathring{\mathbf{B}}) = -\boldsymbol{\Lambda}\cdot(\mathring{\mathbf{B}} - e^2\mathring{B}_z\mathbf{1}_z)$, but this is the toroidal equation in the exterior (2.25)(a).

6 Conclusion

The method described in §3 applies to mean field dynamos with a rank-2 tensor $\boldsymbol{\alpha}$-effect, which are more relevant to galactic dynamo models. The magnetic induction equation (2.11)(a) becomes

$$\partial_t\mathring{\mathbf{B}} = \left(\mathring{\nabla}^2 + \frac{e^2}{1-e^2}\partial_{\mathring{z}\mathring{z}}\right)\mathring{\mathbf{B}} + \mathring{R}_{\mathrm{m}}\mathring{\nabla}\times(\mathring{\mathbf{v}}\times\mathring{\mathbf{B}}) + \mathring{R}_\alpha\mathbf{L}\cdot\mathring{\nabla}\cdot(\mathbf{L}\times\boldsymbol{\alpha}\cdot\mathbf{L}^{-1}\cdot\mathring{\mathbf{B}})\,.$$

The method also applies directly to the kinematic dynamo problem in prolate spheroids, and extends easily to tri-axial ellipsoids and to homeoidal ellipsoidal shells (using vector and tensor spherical harmonics). The method can also be applied to thermal convection and magnetoconvection problems. For non-homeoidal shells such as confocal shells, non-homeoidal toroidal-poloidal fields are required, but derivation of the toroidal-poloidal spectral equations is more difficult (for the confocal case see Schmitt, 2006, Schmitt and Jault, 2004). Work on time-stepping the kinematic dynamo problem is in progress.

References

A.A. Bachtiar and R.W. James. Dynamo convergence tests, and application to a planar velocity dynamo. *Geophys. Astrophys. Fluid Dynam.*, 104:531–543, 2010. doi: 10.1080/03091929.2010.510797.

G.H. Bryan. The waves on a rotating liquid spheroid of finite ellipticity. *Phil. Trans. Roy. Soc. Lond. A*, 180:187–219, 1889.

E. C. Bullard and H. Gellman. Homogeneous dynamos and terrestrial magnetism. *Phil. Trans. R. Soc. Lond. A*, 247:213–278, 1954.

U.R. Christensen et al. A numerical dynamo benchmark. *Phys. Earth Planet. Int.*, 128:25–34, 2001.

M.L. Dudley and R.W. James. Time-dependent kinematic dynamos with stationary flows. *Proc. Roy. Soc. Lond. A*, 425:407–429, 1989.

W. M. Elsasser. Induction effects in terrestrial magnetism. part 1. theory. *Phys. Rev.*, 69:106–116, 1946.

T. Emig, N. Graham, R. L. Jaffe, and M. Kardar. Casimir manipulations: The orientation dependence of fluctuation-induced forces. *Phys. Rev. D*, 77, 2008. doi: 10.1093/gji/ggv527.

J. Ernst-Hullermann, H. Harder, and U. Hansen. Finite volume simulations of dynamos in ellipsoidal planets. *Geophys. J. Int.*, 2013. doi: 10.1093/gji/ggt303.

P. E. Falloon, P. C. Abbott, and J. B. Wang. Theory and computation of spheroidal wavefunctions. *J. Phys. A: Math. Gen.*, 36:5477–5495, 2003.

C. Flammer. *Spheroidal Wave Functions*. Dover Publications, New York, 2005.

G.A. Glatzmaier and P.H. Roberts. A three-dimensional convective dynamo with rotating and finitely conducting inner core and mantle. *Phys. Earth Planet. Int.*, 91:63–75, 1995.

D. Gubbins. Numerical solutions of the kinematic dynamo problem. *Phil. Trans. R. Soc. Lond. A*, 274: 493–521, 1973.

D. J. Ivers. Magnetic free-decay modes in spheroids of small ellipticity. *Preprint, School of Mathematics & Statistics, University of Sydney*, 2017.

A. Jackson et al. A spherical shell numerical dynamo benchmark with pseudo-vacuum magnetic boundary conditions. *Geophys. J. Int.*, 196:712–723, 2014. doi: 10.1093/gji/ggt425.

C. A. Jones, P. Boronski, A. S. Brun, G. A. Glatzmaier, T. Gastine, M. S. Miesch, and J. Wicht. Anelastic convection-driven dynamo benchmarks. *Icarus*, 216:120–135, 2011.

C.A. Jones. Planetary magnetic fields and fluid dynamos. *Annu. Rev. Fluid Mech.*, 43:583–614, 2011. doi: 10.1146/annurev-fluid-122109-160727.

A. Kageyama and T. Sato. Computer simulation of a magnetohydrodynamic dynamo. *Phys. Plasmas*, 2: 1421–1431, 1995.

W. Kuang and J. Bloxham. An Earth-like numerical dynamo model. *Nature*, 389:371–374, 1997.

H. Latter and D. Ivers. Spherical single-roll dynamos at large magnetic reynolds numbers. *Phys. Fluids*, 22, 2010. doi: 10.1063/1.3453712.

P. Marti et al. Full sphere hydrodynamic and dynamo benchmarks. *Geophys. J. Int.*, 197:119–134, 2014. doi: 10.1093/gji/ggt518.

H. Matsui et al. Performance benchmarks for a next generation numerical dynamo model. *Geochem. Geophys. Geosyst.*, 17, 2016. doi: 10.1002/2015GC006159.

F. W. J. Olver, D. W. Lozier, R. F. Boisvert, and C. W. Clark. *NIST Handbook of Mathematical Functions*. Cambridge University Press, New York, 2010.

C. L. Pekeris, Y. Accad, and B. Shkoller. Kinematic dynamos and the earth's magnetic field. *Phil. Trans. R. Soc. Lond. A*, 275:425–461, 1973.

C.G. Phillips and D.J. Ivers. Spherical anisotropic diffusion models for the Earth's core. *Phys. Earth Planet. Int.*, 117:209–223, 2000.

C.G. Phillips and D.J. Ivers. Strong field anisotropic diffusion models for the Earth's core. *Phys. Earth Planet. Int.*, 140:13–28, 2003.

H. Poincaré. Sur l'équilibre d'une masse fluide animée d'un mouvement de rotation. *Acta Math.*, 7:259–380, 1885.

M. H. Protter and H. F. Weinberger. *Maximum Principles in Differential Equations*. Springer-Verlag, New York, 1984.

D. Schmitt. Numerical study of viscous modes in a rotating spheroid. *J. Fluid Mech.*, 567:399–414, 2006.

D. Schmitt and D. Jault. Numerical study of a rotating fluid in a spheroidal container. *J. Comput. Phys.*, 197:671–685, 2004.

A. M. Soward. A thin disc model of the galactic dynamo. *Astron. Nachr.*, 299:25–33, 1978.

M. Stix. The galactic dynamo. *Astron & Astrophys*, 42:85–89, 1975.

S. Vantieghem, A. Sheyko, and A. Jackson. Applications of a finite-volume algorithm for incompressible MHD problems. *Geophys. J. Int.*, 204:1376–1395, 2016. doi: 10.1093/gji/ggv527.

M. P. White. Numerical models of the galactic dynamo. *Astron. Nachr.*, 299:209–216, 1978.

C.-C. Wu and P. H. Roberts. On a dynamo driven by topographic precession. *Geophys. Astrophys. Fluid Dynam.*, 103:467–501, 2009. doi: 10.1080/03091920903311788.

Appendix A The Horizontal Spectral Equations

The horizontal divergence equations in the conducting region and insulating exterior contain no new information. The spectral form of the horizontal divergence of the magnetic induction equation in the conducting region is $\mathrm{d}_1(\partial_{\mathring{t}} - \mathrm{D}_n)S_n^m = \mathcal{H}_n^m\{\mathbf{F}\}$, where the operator $\mathrm{d}_1 := \mathrm{d}_r + r^{-1}$, $\mathbf{F} = e^2\partial_{\mathring{z}\mathring{z}}\mathring{\mathbf{B}}/(1-e^2) + R_\mathrm{m}\mathring{\nabla}\times(\mathring{\mathbf{v}}\times\mathring{\mathbf{B}})$ and $\mathcal{H}_n^m$ is defined by (5.8). The anisotropic magnetic diffusion term is $\mathcal{H}_n^m\{\partial_{\mathring{z}\mathring{z}}\mathbf{B}\} = \mathrm{d}_1 L_n^m(T,S)$. In fact, the equation is simply d_1 applied to the radial induction equation (2.23).

In the insulating region $r\mathring{\nabla}_\mathrm{h}\cdot(\mathring{\nabla}\times\mathbf{B})_\mathrm{h} = r^{-1}(r\mathring{\nabla}_\mathrm{h}\cdot)^2\partial_r(rT) = -\mathrm{d}_1\sum_{n,m}\lambda_n T_n^m Y_n^m$ and

$$r\mathring{\nabla}_\mathrm{h}\cdot(\mathring{\nabla}\times B_z\mathbf{1}_z)_\mathrm{h} = -\mathrm{d}_1\sum_{n,m} im\{-(n-1)c_n^m \mathrm{d}_{1-n}S_{n-1}^m + (n+2)c_{n+1}^m \mathrm{d}_{n+2}S_{n+1}^m - imT_n^m\}Y_n^m\,.$$

Thus, $r\mathring{\nabla}_\mathrm{h}\cdot\{\mathring{\nabla}\times(\mathbf{B} - e^2B_z\mathbf{1}_z)\}_\mathrm{h} = 0$ is equivalent to applying the operator d_1 to the toroidal equation (2.25)(a) in the exterior.

Appendix B Angular Spectral Forms of the Induction Term

The induction term expansions (B1) and (B2) are derived in Bullard and Gellman (1954) (with an additional factor of r in the toroidal and poloidal potentials),

$$\mathcal{R}_\gamma\{\nabla\times(\mathbf{v}\times\mathbf{B})\} = \sum_{\alpha,\beta}\{(s_\alpha S_\beta S_\gamma) + (s_\alpha T_\beta S_\gamma) + (t_\alpha S_\beta S_\gamma) + (t_\alpha T_\beta S_\gamma)\}\,, \tag{B1}$$

$$\begin{aligned}
(s_\alpha S_\beta S_\gamma) &:= \tfrac{1}{2}A_{\alpha\beta\gamma^*}\{-\lambda_\alpha\lambda_{\bar\alpha\beta\gamma}s_\alpha(rS_\beta)' + \lambda_\beta\lambda_{\alpha\bar\beta\gamma}(rs_\alpha)'S_\beta\}/r^2\\
(s_\alpha T_\beta S_\gamma) &:= E_{\alpha\beta\gamma^*}\lambda_\alpha s_\alpha T_\beta/r\\
(t_\alpha S_\beta S_\gamma) &:= E_{\alpha\beta\gamma^*}\lambda_\beta t_\alpha S_\beta/r\\
(t_\alpha T_\beta S_\gamma) &:= 0\,.
\end{aligned}$$

where primes indicate radial derivatives, $\lambda_\alpha := \alpha(\alpha+1)$, $\lambda_{\alpha\beta\gamma} := \lambda_\alpha + \lambda_\beta + \lambda_\gamma$, $\lambda_{\alpha\bar\beta\gamma} := \lambda_\alpha - \lambda_\beta + \lambda_\gamma$, etc and

$$\mathcal{T}_\gamma\{\nabla\times(\mathbf{v}\times\mathbf{B})\} = \sum_{\alpha,\beta}\{(s_\alpha S_\beta T_\gamma) + (s_\alpha T_\beta T_\gamma) + (t_\alpha S_\beta T_\gamma) + (t_\alpha T_\beta T_\gamma)\}\,, \tag{B2}$$

$$\begin{aligned}
(s_\alpha S_\beta T_\gamma) &:= \tfrac{1}{2}E_{\alpha\beta\gamma^*}\{\lambda_{\alpha\beta\gamma}s_\alpha S_\beta - \lambda_{\alpha\beta\bar\gamma}[r(s_\alpha S_\beta)' + r^2 s_\alpha' S_\beta'] - \lambda_\alpha r^2 s_\alpha S_\beta'' - \lambda_\beta r^2 s_\alpha'' S_\beta\}/r^3\\
(s_\alpha T_\beta T_\gamma) &:= \tfrac{1}{2}A_{\alpha\beta\gamma^*}\{-\lambda_\gamma\lambda_{\alpha\beta\bar\gamma}(s_\alpha T_\beta + rs_\alpha' T_\beta) - \lambda_\alpha\lambda_{\bar\alpha\beta\gamma}(rs_\alpha' T_\beta + rs_\alpha T_\beta')\}/r^2\\
(t_\alpha S_\beta T_\gamma) &:= A_{\alpha\beta\gamma^*}\{\lambda_\gamma\lambda_{\alpha\beta\bar\gamma}(t_\alpha S_\beta + rt_\alpha S_\beta') + \lambda_\beta\lambda_{\alpha\bar\beta\gamma}(rt_\alpha' S_\beta + rt_\alpha S_\beta')\}/r\\
(t_\alpha T_\beta T_\gamma) &:= \lambda_\gamma E_{\alpha\beta\gamma^*}t_\alpha T_\beta/r\,.
\end{aligned}$$

The Adams-Gaunt integral $A^{m_\alpha m_\beta m_\gamma}_{n_\alpha\, n_\beta\, n_\gamma}$ and Elsasser dynamo integral $E^{m_\alpha m_\beta m_\gamma}_{n_\alpha\, n_\beta\, n_\gamma}$ are defined by

$$A^{m_\alpha m_\beta m_\gamma}_{n_\alpha\, n_\beta\, n_\gamma} := \frac{1}{4\pi}\oint Y^{m_\alpha}_{n_\alpha} Y^{m_\beta}_{n_\beta} Y^{m_\gamma}_{n_\gamma}\,\mathrm{d}\mathring{\Omega}$$

$$E^{m_\alpha m_\beta m_\gamma}_{n_\alpha\, n_\beta\, n_\gamma} := \frac{1}{4\pi}\int_0^{2\pi}\int_0^{\pi} (\partial_\theta Y^{m_\alpha}_{n_\alpha}\,\partial_\phi Y^{m_\beta}_{n_\beta} - \partial_\phi Y^{m_\alpha}_{n_\alpha}\,\partial_\theta Y^{m_\beta}_{n_\beta}) Y_\gamma\,\mathrm{d}\theta\,\mathrm{d}\phi\,,$$

In terms of $3j$-symbols,

$$A_{\alpha\beta\gamma} = \Lambda(\alpha,\beta,\gamma)\begin{pmatrix} n_\alpha & n_\beta & n_\gamma \\ 0 & 0 & 0\end{pmatrix}\begin{pmatrix} n_\alpha & n_\beta & n_\gamma \\ m_\alpha & m_\beta & m_\gamma\end{pmatrix}$$

$$E_{\alpha\beta\gamma} = -i\Lambda(\alpha,\beta,\gamma)\Delta(\alpha,\beta,\gamma)\begin{pmatrix} n_\alpha+1 & n_\beta+1 & n_\gamma+1 \\ 0 & 0 & 0\end{pmatrix}\begin{pmatrix} n_\alpha & n_\beta & n_\gamma \\ m_\alpha & m_\beta & m_\gamma\end{pmatrix},$$

where

$$\Delta(\alpha,\beta,\gamma) = \sqrt{\frac{(n_{\alpha\beta\gamma}+2)(n_{\alpha\beta\gamma}+4)}{4(n_{\alpha\beta\gamma}+3)}}\sqrt{(n_{\bar\alpha\beta\gamma}+1)(n_{\alpha\bar\beta\gamma}+1)(n_{\alpha\beta\bar\gamma}+1)}\,.$$

with $n_{\alpha\beta\gamma} := n_\alpha + n_\beta + n_\gamma$, $n_{\alpha\bar\beta\gamma} := n_\alpha - n_\beta + n_\gamma$, etc.

Appendix C Axisymmetric free-decay rates

c/a	$\mathring{\gamma}^{\mathrm{m}}_{1,1}c/a$	$\mathring{\gamma}^{\mathrm{m}}_{1,2}c/a$	$\mathring{\gamma}^{\mathrm{a}}_{1,1}(c/a)^2$	$\mathring{\gamma}^{\mathrm{a}}_{1,2}(c/a)^2$	$\mathring{\gamma}^{\mathrm{a}}_{2,1}(c/a)^2$	$\mathring{\gamma}^{\mathrm{a}}_{3,1}(c/a)^2$
1.00	9.869604401	20.190728556	20.190728556	59.679515944	33.217461914	48.831193644
0.95	9.573463520	20.055037754	18.613749809	55.143044929	31.359968460	46.156321167
0.90	9.277209597	19.938272263	17.113443397	51.154471585	29.583789242	43.268233071
0.85	8.980829306	19.843715162	15.689963175	47.785740476	27.888848717	40.094806581
0.80	8.684306079	19.775447577	14.343430635	44.987859397	26.274897455	36.684608046
0.75	8.387619214	19.738608214	13.073916808	42.616368122	24.741463026	33.181370561
0.70	8.090742726	19.739761920	11.881417136	40.534934346	23.287792006	29.720337242
0.65	7.793643821	19.787435038	10.765816420	38.654989408	21.912783614	26.388556676
0.60	7.496280891	19.892913332	9.726839734	36.924907840	20.614917500	23.235623972
0.55	7.198600817	20.071466941	8.763983471	35.314099582	19.392181612	20.289491743
0.50	6.900535321	20.344296723	7.876418810	33.803139044	18.242011186	17.566210599
0.45	6.601995965	20.741754519	7.062858522	32.378570791	17.161256187	15.074925162
0.40	6.302867166	21.308935269	6.321380045	31.030259621	16.146199525	12.820193872
0.35	6.002996288	22.115977381	5.649209918	29.750035017	15.192646483	10.802780638
0.30	5.702179241	23.278482385	5.042510539	28.530990811	14.296089721	9.019441606
0.25	5.400138973	25.002008642	4.496284019	27.367114899	13.451922975	7.462044036
0.20	5.096492218	27.692128802	4.004589491	26.253081717	12.655647658	6.116720679
0.15	4.790695731	29.213416496	3.561191068	25.184123285	11.903020017	4.964576007
0.10	4.481954125	41.511793699	3.160335450	24.155938651	11.190124920	3.984883255
0.09	4.419755597	44.576686595	3.084822548	23.954844700	11.051993860	3.807895437
0.08	4.357380346	48.394890704	3.010777197	23.755194930	10.915281480	3.636879220
0.07	4.294814582	53.282588634	2.938165403	23.556960350	10.779961450	3.471693435
0.06	4.232043027	59.763884660	2.866954338	23.360112471	10.646007969	3.312200030
0.05	4.169048686	68.776654491	2.797112297	23.164623292	10.513395759	3.158263906
0.04	4.105812582	82.184711526	2.728608657	22.970465280	10.382100054	3.009752757
0.03	4.042313418	104.306446505	2.661413830	22.777611361	10.252096592	2.866536917
0.02	3.978527174	143.485205010	2.595499228	22.586034899	10.123361606	2.728489210
0.01	3.914426594	266.247562876	2.530837220	22.651011290	9.995871812	2.595484809

Table 3: Axisymmetric meridional $\mathring{\gamma}^{\mathrm{m}}_{nk}$ and azimuthal $\mathring{\gamma}^{\mathrm{a}}_{nk}$ growth rates with weights c/a and $(c/a)^2$ for $0.01 \le c/a \le 1$.